Exploring the consequences of redirecting an exocytic Rab onto endocytic vesicles

Xia Li[a], Dongmei Liu[a], Eric Griffis[b], and Peter Novick[a,*]
[a]Department of Cellular and Molecular Medicine, University of California, San Diego, La Jolla, CA 92093-0644;
[b]Nikon Imaging Center, University of California, San Diego, La Jolla, CA 92093-0694

ABSTRACT **Bidirectional vesicular traffic links compartments along the exocytic and endocytic pathways. Rab GTPases have been implicated in specifying the direction of vesicular transport. To explore this possibility, we sought to redirect an exocytic Rab, Sec4, onto endocytic vesicles by fusing the catalytic domain of the Sec4 GEF, Sec2, onto the CUE localization domain of Vps9, a GEF for the endocytic Rab Ypt51. The Sec2GEF-GFP-CUE construct localized to bright puncta predominantly near sites of polarized growth, and this localization was dependent on the ability of the CUE domain to bind to the ubiquitin moieties added to the cytoplasmic tails of proteins destined for endocytic internalization. Sec4 and Sec4 effectors were recruited to these puncta with various efficiencies. Cells expressing Sec2GEF-GFP-CUE grew surprisingly well and secreted protein at near-normal efficiency, implying that Golgi-derived secretory vesicles were delivered to polarized sites of cell growth despite the misdirection of Sec4 and its effectors. A low efficiency mechanism for localization of Sec2 to secretory vesicles that is independent of known cues might be responsible. In total, the results suggest that while Rabs may play a critical role in specifying the direction of vesicular transport, cells are remarkably tolerant of Rab misdirection.**

Monitoring Editor
Bruno Goud
Institut Curie

Received: Feb 1, 2023
Accepted: Feb 22, 2023

INTRODUCTION

Organelles along membrane transport pathways are linked by extensive, bidirectional, vesicular traffic. A key question is how the direction of any given vesicle is determined. Integral membrane proteins required for membrane fusion, such as the vesicle SNAREs, cycle continuously through both anterograde and retrograde vesicles (Lewis *et al*., 2000) and therefore appear to be ill suited to specify the direction of vesicle traffic (Whyte and Munro, 2002). In contrast, Rab GTPase activation and membrane association is reversible, with different Rabs tagging anterograde and retrograde vesicles. Thus Rabs appear to be better equipped to specify the direction of vesicle transport (Mizuno-Yamasaki *et al*., 2012). Rab activation requires a guanine nucleotide exchange factor (GEF), and Rab inactivation by GTP hydrolysis requires a GTPase-activating protein (GAP). GDP-bound, lipid-anchored Rabs are subject to extraction from membranes by Rab GDP dissociation inhibitor (GDI) (Araki *et al*., 1990). By locating a GEF on one compartment and a GAP on another compartment, an asymmetric, unidirectional Rab distribution can be established. Rab effectors are defined by their recognition of a specific GTP-bound Rab and constitute a diverse collection of molecules that includes molecular motors that drive the vectorial delivery of an organelle or vesicular carrier along a cytoskeletal track, tethers that mediate the initial recognition of the target compartment by a vesicular carrier, and SNARE regulators that control the assembly of specific SNARE complexes and their function in membrane fusion (Grosshans *et al*., 2006b). As a membrane flows along the exocytic or endocytic pathways, the Rabs associated with that membrane change, and as each new Rab decorates the membrane, it recruits a distinct set of effectors that help to define the functional identity of the membrane with which it is associated.

Rabs represent the largest branch of the GTPase superfamily, with more than 60 members in mammals and 10 in yeast (Seabra *et al*., 2002). Reflecting the importance of Rabs as key nodes in the regulation of membrane traffic, a wide variety of human diseases have been attributed to defects in Rab expression, Rab prenylation,

This article was published online ahead of print in MBoC in Press (http://www.molbiolcell.org/cgi/doi/10.1091/mbc.E23-01-0037) on March 1, 2023.

*Address correspondence to: Peter Novick (pnovick@ucsd.edu).

Abbreviations used: ADH1, alcohol dehydrogenase 1; DIC, differential interference contrast; ER, endoplasmic reticulum; ESCRT, endosomal sorting complex required for transport; FRAP, fluorescence recovery after photobleaching; RAB, Ras-associated binding; SEM, standard error of the mean; tSNARE, target membrane soluble *N*-ethylmaleimide-sensitive factor activating protein receptor; vSNARE, vesicles soluble *N*-ethylmaleimide-sensitive factor activating protein receptor.

Rab GDI, Rab GEFs, Rab GAPs, and Rab effectors (Seabra *et al.*, 2002; Hutagalung and Novick, 2011). Furthermore, a number of clinically important human pathogens exploit and disrupt our Rab regulatory pathways to promote their own intracellular agenda and to evade host defenses (Hutagalung and Novick, 2011).

Different Rabs are often networked to one another through their GEFs, GAPs, and effectors, thereby generating regulatory circuits that can coordinate the various biochemical steps of each individual stage of membrane traffic and link together the stages of an entire transport pathway (Mizuno-Yamasaki *et al.*, 2012). GEF and GAP cascades have been identified in which one Rab recruits the GEF that activates the downstream Rab and/or the GAP that inactivates the upstream Rab (Ortiz *et al.*, 2002; Rivera-Molina and Novick, 2009; Zhu *et al.*, 2009; Pusapati *et al.*, 2012; Suda *et al.*, 2013; Rana *et al.*, 2015). These two cascade mechanisms can work in a countercurrent manner to direct a programmed series of Rab transitions as membrane flows along a membrane traffic pathway. In addition, positive-feedback loops are formed through the ternary interactions of a Rab GEF, the activated Rab, and one of its effectors (Horiuchi *et al.*, 1997; Medkova *et al.*, 2006). These positive-feedback loops can function to sharpen Rab transitions and contribute to the maturation of carrier vesicles (Mizuno-Yamasaki *et al.*, 2010; Stalder *et al.*, 2013).

A key question concerns the importance of these regulatory mechanisms to membrane traffic in vivo. Prior efforts have disrupted individual regulatory elements (Ortiz *et al.*, 2002; Rivera-Molina and Novick, 2009; Nottingham *et al.*, 2012; Pusapati *et al.*, 2012) or redirected a Rab regulatory component to an irrelevant target such as mitochondria (Blumer *et al.*, 2013), but have not attempted to rewire a Rab regulatory circuit within the context of a functioning pathway and then assess the ramifications for membrane traffic. Here we seek to directly test the hypothesis that Rabs dictate the direction of vesicular transport. Our approach has been to fuse the catalytic GEF domain that activates the final Rab of the yeast exocytic pathway with a domain that normally serves to recruit the GEF for the first Rab of the endocytic pathway onto compartments of the endocytic pathway. Because the location of a GEF determines to a large extent where its substrate Rab can stably associate with membranes, this should have the effect of redirecting an exocytic Rab onto endocytic compartments.

Sec2, the exocytic GEF that we sought to redirect, activates Sec4, a Rab8 homologue that serves as the final Rab of the yeast secretory pathway (Walch-Solimena *et al.*, 1997). The catalytic GEF domain near the amino terminus of Sec2 (amino acids [aa] 1–160) forms a homodimeric coiled-coil structure (Dong *et al.*, 2007), while downstream regions are involved in its recruitment to Golgi-derived secretory vesicles through interactions with the upstream Rab Ypt32-GTP (Ortiz *et al.*, 2002), downstream effector Sec15 (Medkova *et al.*, 2006), and the phosphoinositide PI(4)P (Mizuno-Yamasaki *et al.*, 2010). Once activated, Sec4-GTP recruits Myo2, a type V myosin (Walch-Solimena *et al.*, 1997; Jin *et al.*, 2011). This leads to the movement of secretory vesicles along actin cables toward sites of polarized cell growth, including the tips of small buds and the necks separating large buds from the mother cell near the time of cytokinesis (Donovan and Bretscher, 2015). Sec4 also recruits the exocyst complex that tethers secretory vesicles to the plasma membrane (Salminen and Novick, 1989; Guo *et al.*, 1999) and the SNARE regulator Sro7 that promotes exocytic fusion (Grosshans *et al.*, 2006a).

To redirect the GEF domain of Sec2, we fused it to the CUE domain of Vps9, a GEF that activates Ypt51, a Rab5 homologue that serves as the first Rab of the endocytic pathway (Hama *et al.*, 1999). The CUE domain of Vps9 binds to ubiquitin moieties that are added to the cytoplasmic tails of cell surface proteins destined for internalization into endocytic vesicles (Shideler *et al.*, 2015). While the isolated CUE domain can act as a localization domain, recruitment of full-length Vps9 might involve an additional interaction with Arf1-GTP (Nagano *et al.*, 2019). Membrane recruitment of Vps9 is thought to occur at the *trans*-Golgi network (TGN), which appears to play the role of the early endosome in yeast (Day *et al.*, 2018; Nagano *et al.*, 2019). Vesicles carrying Vps9 and endocytic cargo bud from the TGN and are directed to the late endosome (Nagano *et al.*, 2019). Activation of Ypt51 promotes delivery of endocytic cargo to late endosomes where cell surface proteins are deubiquitinated and incorporated into luminal vesicles through the action of the ESCRT complex, forming multivesicular bodies. Following fusion of the multivesicular bodies with the vacuole, the luminal vesicles are degraded. Here we examine the effects of expressing a fusion protein consisting of the GEF domain of Sec2 and the CUE domain of Vps9.

RESULTS

Sec2GEF-GFP-CUE localizes to bright, focused puncta dependent on the ubiquitin-binding activity of the CUE domain

To explore the effects of replacing the normal localization domain of Sec2 with that of Vps9, we fused the GEF domain (aa 1–160) of Sec2 to GFP and then to the CUE domain of Vps9 (aa 408–450), generating Sec2GEF-GFP-CUE. Unless otherwise indicated, we expressed this construct from the *ADH1* promoter as the sole copy of Sec2, with or without the M419D CUE domain mutation that blocks binding to ubiquitin (Shideler *et al.*, 2015). As controls, we expressed full-length Sec2 fused to GFP (Sec2-GFP) and the GEF domain alone fused to GFP (Sec2GEF-GFP). As previously shown (Elkind *et al.*, 2000), Sec2-GFP exhibited concentrations at the tips of small buds or across the necks of large budded cells, reflecting its association with secretory vesicles (Figure 1A). Sec2GEF-GFP, lacking the Ypt32, Sec15, and PI(4)P binding sites that serve to recruit Sec2 to secretory vesicles, was predominantly cytosolic; nonetheless ~30% of the cells exhibited detectable, bud tip or neck localization. This residual localization likely reflects its association with Sec4 on secretory vesicles as the percentage increased to ~50% upon Sec4 overexpression (Figure 1B). Sec2GEF-GFP-CUE exhibited several bright, tightly focused puncta per cell as well as numerous dimmer puncta and little cytosolic background. The bright puncta were frequently near sites of polarized cell surface expansion. However, the puncta within buds were often closer to the sides of the buds rather than at the tips, and localization at necks was in the form of a focused punctum rather than a bar across the neck. Sec2GEF-GFP-CUE^{M419D} showed largely cytosolic localization with no concentration other than a slightly higher fluorescence of the nucleus relative to the cytoplasm (Figure 1A). A minor fraction of cells expressing Sec2GEF-GFP-CUE^{M419D} exhibited polarized fluorescence and, as in the case of Sec2GEF-GFP, this percentage increased in cells overexpressing Sec4 (Figure 1B). Together, these data indicate that the CUE domain serves to efficiently localize Sec2GEF-GFP-CUE and that this function relies on its ability to interact with ubiquitin. The localization is distinct from that of full-length Sec2; nonetheless many structures bearing Sec2GEF-GFP-CUE localize relatively close to the normal sites of cell surface growth despite their abnormally punctate appearance. Similar results were observed with constructs employing mCherry or NeonGreen as fluorescent tags (see below).

Movies were made using constructs containing the more-photostable NeonGreen variant. These revealed that the bright Sec2GEF-NeonGreen-CUE puncta were largely static, showing little movement over a 30 s time frame. Dimmer puncta were more mobile but did not exhibit directed movement, and most persisted over the

30 s observation period (Figure 1C and Supplemental Movie S1). In contrast, Sec2-NeonGreen structures were more dynamic, and many smaller puncta displayed rapid, directed movement toward bud tips or bud necks. These persisted for an average of only 5 s (Figure 1C and Supplemental Movie S2). The dynamic localization of Sec2 reflects its association with secretory vesicles that fuse with the plasma membrane soon after delivery by Myo2 on actin cables (Elkind *et al.*, 2000; Donovan and Bretscher, 2015).

While individual vesicles carrying fluorescently tagged proteins could be tracked, they became challenging to follow once they entered the bud due to the existing pool of vesicles at sites of polarized growth. Photobleaching all signals from existing vesicles in the bud allowed better visualization of new vesicles entering the bud from the mother cell. The experimental condition used for photobleaching the entire bud with a 405-nm laser did not affect cell growth, suggesting that the bleach event was not disturbing essential processes in exocytosis. After photobleaching the entire small bud, the rate of recovery of Sec2GEF-NeonGreen-CUE was similar to that of Sec2-NeonGreen, but less total signal was recovered in Sec2GEF-NeonGreen-CUE cells (Figure 1D and Supplemental Movies S3 and S4). Thus, although the bright Sec2GEF-GFP-CUE puncta appear static, additional Sec2GEF-GFP-CUE protein can be recruited to preexisting puncta.

To quantitate the time of residence of individual vesicles at the plasma membrane before fusion, we photobleached the bud and then followed delivery of vesicles from the unbleached region of the cell to the bud tip. We documented events in which the initial vesicle immobilization at the cell cortex was observed and the subsequent disappearance was seen in one of the three middle imaging planes, thereby excluding events in which the vesicle moved out of the focal plane (Figure 1E, left panel). Most vesicles carrying Sec2-NeonGreen (70%) remained stationary at the cell cortex for less than 10 s before they disappeared (Figure 1E and Supplemental Movie S5). In cells expressing Sec2GEF-NeonGreen-CUE there were fewer puncta and 60% of them remained stationary for longer than 20 s, suggesting a delay after tethering and before fusion (Figure 1E and Supplemental Movie S6).

Sec2GEF-CUE is efficiently recruited to the enlarged late endosomes in *vps4*Δ cells

Because the punctate localization of Sec2GEF-GFP-CUE was largely dependent on the ubiquitin-binding activity of its Vps9-derived CUE domain, we anticipated that it would colocalize with endogenous Vps9. About half of the Sec2GEF-GFP-CUE puncta were positive for Vps9-mCherry, regardless of their position within the cell, while Sec2-GFP displayed almost no colocalization with Vps9-mCherry (Supplemental Figure S1). The ubiquitin moiety on endocytic cargo usually remains accessible to the cytoplasm for only a short time before the cargo is deubiquitinated and incorporated into luminal vesicles in late endosomes by the ESCRT machinery (Shideler *et al.*, 2015). The transient nature of CUE binding sites results in a high cytoplasmic background of Vps9-mCherry, which could explain the incomplete colocalization of Sec2GEF-GFP-CUE and Vps9-mCherry. We reexamined the colocalization in a *vps4*Δ mutant. In this ESCRT-defective mutant, ubiquitinated cargo remains exposed to the cytoplasm on the surface of an enlarged late endosome, termed a "class E" compartment, leading to enhanced recruitment of Vps9 and a reduction in the cytoplasmic pool (Shideler *et al.*, 2015). Sec2GEF-GFP-CUE localized to additional puncta at nonpolarized sites in *vps4*Δ cells (Supplemental Figure S2A). Most of the Sec2GEF-GFP-CUE puncta at both polarized and nonpolarized sites were also labeled with Vps9-mCherry, while Sec2-GFP structures were not positive for Vps9-mCherry (Figure 2A). Vps9 serves to recruit and activate the Rab5 homologue Ypt51 on endosomes (Hama *et al.*, 1999). We observed extensive colocalization of mCherry-Ypt51 with Sec2GEF-GFP-CUE at both polarized and nonpolarized sites in *vps4*Δ cells (Figure 2B). No colocalization was observed with Sec2-GFP. We also observed substantial colocalization of the late endosome marker Vps8-mCherry with Sec2GEF-GFP-CUE, but not with Sec2-GFP in *vps4*Δ cells (Figure 2C). Thus, the CUE domain serves to efficiently recruit Sec2GEF-GFP-CUE to endocytic membranes.

We also asked whether the enlarged late endosomes bearing Sec2GEF-GFP-CUE or Sec2GEF-mCherry-CUE in *vps4*Δ cells recruit Sec4 and Sec4 effectors. We observed nearly complete colocalization of GFP-Sec4 and Sec2GEF-mCherry-CUE at both polarized or nonpolarized sites in *vps4*Δ cells, while colocalization of GFP-Sec4 and Sec2-mCherry was mainly at polarized sites (Supplemental Figure S2B). There was extensive colocalization of Myo2-GFP and Sec2GEF-mCherry-CUE or Sec8-mCherry and Sec2GEF-GFP-CUE at polarized sites in *vps4*Δ cells (Figure 2D and Supplemental Figure S2C). However, at nonpolarized sites there was only partial colocalization of Myo2-GFP and Sec2GEF-mCherry-CUE (Figure 2D) and no colocalization of Sec8-mCherry with Sec2GEF-GFP-CUE (Supplemental Figure S2C). No colocalization of the Golgi marker, Sec7-dsRed, was seen with either Sec2GEF-GFP-CUE or Sec2-GFP in *vps4*Δ cells (Supplemental Figure S2D). The observation that most of the compartments formed in response to Sec2GEF-CUE expression in *vps4*Δ cells bear both endosomal markers and secretory vesicle markers indicates that Sec2GEF-CUE is efficiently recruited to endosomal membranes in these cells and suggests that these compartments have a mixed identity.

Because the vesicle clusters marked by Sec2GEF-GFP-CUE had some characteristics of both an exocytic compartment and an endocytic compartment, we explored whether they would be marked by PI(4)P, the phosphoinositide made in the TGN, or PI(3)P, the phosphoinositide made in early endosomes. Neither Sec2-GFP nor Sec2GEF-GFP-CUE colocalized to a large degree with mCherry-FAPP1-PH, a probe for PI(4)P, in either a *VPS4* background or a *vps4*Δ background (Supplemental Figure S3, A and B). Sec2-GFP exhibited no colocalization with mRFP-FYVE(EEA1), a probe for PI(3)P in either a *VPS4* background or a *vps4*Δ background (Supplemental Figure S3, C and D). While Sec2GEF-GFP-CUE did not colocalize significantly with mRFP-FYVE(EEA1) in a *VPS4* background, ~30% of the Sec2GEF-GFP-CUE puncta did colocalize with mRFP-FYVE(EEA1) in a *vps4*Δ background. Colocalization was observed at both polarized and nonpolarized sites (Supplemental Figure S3, C and D).

Sec2GEF-CUE can recruit Sec4 and Sec4 effectors to polarized sites but is less efficient in the recruitment of effectors to nonpolarized sites

Because we observed extensive colocalization of GFP-Sec4 and Sec2GEF-mCherry-CUE at both polarized and nonpolarized sites in *vps4*Δ cells, we examined GFP-Sec4 in *VPS4* cells expressing Sec2GEF-mCherry-CUE or Sec2-mCherry. Nearly all Sec2GEF-mCherry-CUE puncta were also labeled with GFP-Sec4 whether they were near sites of polarized growth or at nonpolarized sites. In control cells expressing Sec2-mCherry, both proteins were found predominantly at polarized sites (Figure 3A). These results are consistent with the observation that Rab GEFs can recruit their substrate Rabs to ectopic sites (Blumer *et al.*, 2013).

Activation of Sec4 by Sec2GEF-GFP-CUE is also expected to lead to colocalization with downstream Sec4 effectors. The exocyst is normally recruited to secretory vesicles through

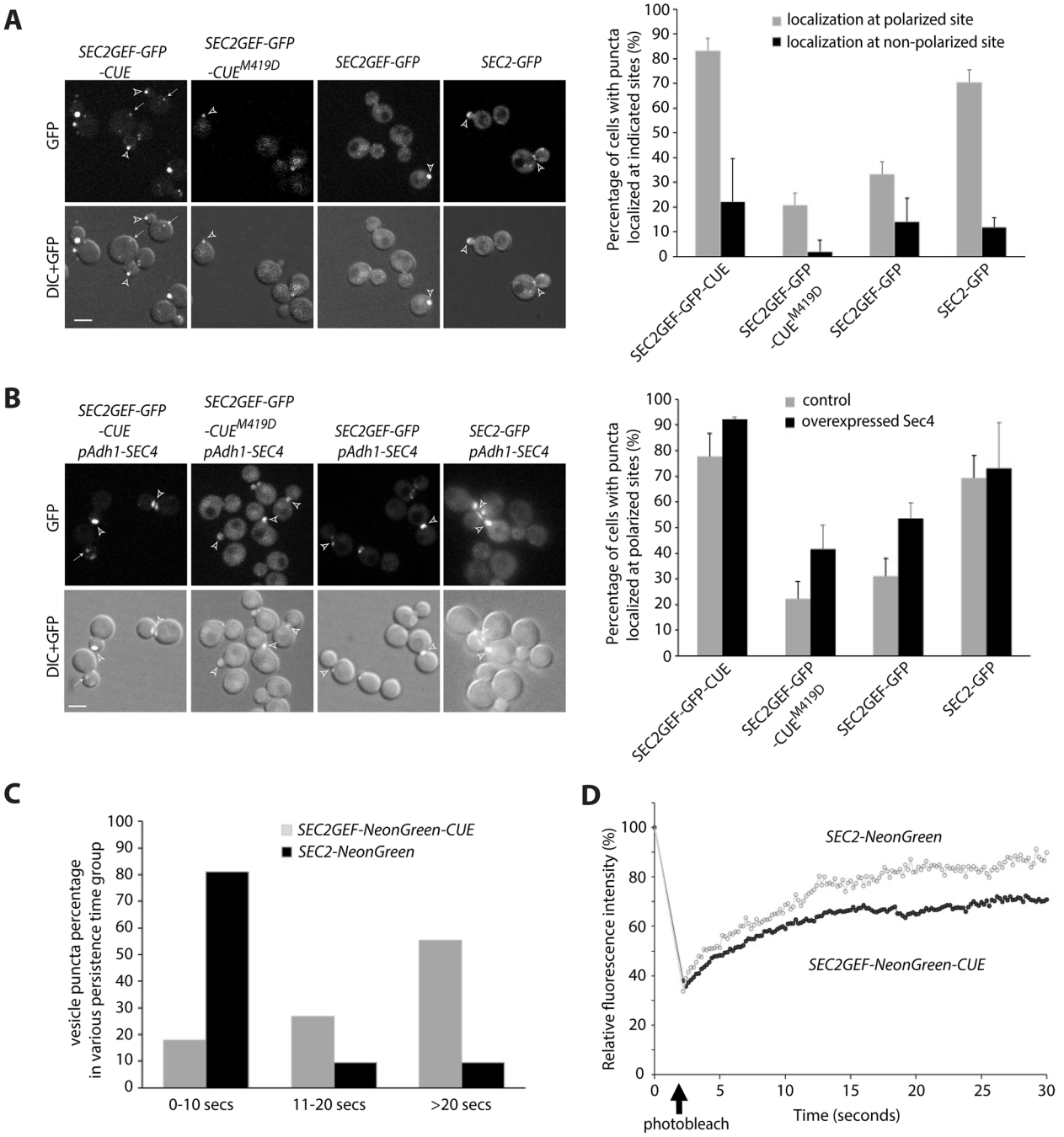
A
SEC2GEF-GFP -CUE
SEC2GEF-GFP -CUE^M419D
SEC2GEF-GFP
SEC2-GFP
GFP
DIC+GFP
localization at polarized site
localization at non-polarized site
Percentage of cells with puncta localized at indicated sites (%)
SEC2GEF-GFP-CUE
SEC2GEF-GFP -CUE^M419D
SEC2GEF-GFP
SEC2-GFP
B
SEC2GEF-GFP -CUE pAdh1-SEC4
SEC2GEF-GFP -CUE^M419D pAdh1-SEC4
SEC2GEF-GFP pAdh1-SEC4
SEC2-GFP pAdh1-SEC4
control
overexpressed Sec4
C
SEC2GEF-NeonGreen-CUE
SEC2-NeonGreen
vesicle puncta percentage in various persistence time group
0-10 secs
11-20 secs
>20 secs
D
SEC2-NeonGreen
SEC2GEF-NeonGreen-CUE
Relative fluorescence intensity (%)
photobleach
Time (seconds)
E
frame-to-frame disappearance
tethering
last frame
fusion
SEC2-NeonGreen
pre-bleach
bleach
5 sec
7 sec
9 sec
12 sec
14 sec
SEC2GEF-NeonGreen-CUE
13 sec
17 sec
21 sec
25 sec
29 sec
33 sec
37 sec
41 sec
45 sec
49 sec
% of vesicle puncta in various persistence time group

interactions of Sec4-GTP with the Sec15 subunit (Salminen and Novick, 1989; Guo *et al.*, 1999). We examined cells coexpressing Sec2GEF-GFP-CUE or Sec2-GFP and the exocyst subunit Sec8-mCherry. In both strains, nearly all the GFP structures at polarized sites were also labeled with Sec8-mCherry; however, the Sec-2GEF-GFP-CUE structures observed at nonpolarized sites were labeled to a lower extent with Sec8-mCherry (Figure 3B). Similar results were observed for cells coexpressing Sec2GEF-GFP-CUE or Sec2-GFP and the exocyst subunit Sec15-mCherry (Supplemental Figure S4A).

Most exocyst subunits are delivered to polarized sites by riding on secretory vesicles along polarized actin cables, while the subunits Sec3 and Exo70 exhibit polarized localization that is partially insensitive to disruption of the actin cytoskeleton (Finger *et al.*, 1998; Boyd *et al.*, 2004; Hutagalung *et al.*, 2009; Liu and Novick, 2014). We examined cells coexpressing Sec2GEF-GFP-CUE or Sec2-GFP and the exocyst subunit Sec3-mCherry. Approximately 40% of Sec2GEF-GFP-CUE puncta were labeled with Sec3-mCherry near sites of polarized growth, while Sec2GEF-GFP-CUE structures observed at nonpolarized sites were labeled to an even lower extent with Sec3-mCherry. In many cells, a Sec2GEF-GFP-CUE punctum was observed directly adjacent to a Sec3-mCherry structure (Supplemental Figure S4C, bottom panel). In control cells expressing Sec2-GFP, both proteins were found well colocalized predominantly at polarized sites (Supplemental Figure S4C). Similar results were observed when we coexpressed Sec2GEF-mCherry-CUE or Sec2-mCherry with Exo70-GFP (Supplemental Figure S4D). These findings indicate that in cells expressing Sec-2GEF-CUE, vesicles are delivered to polarized exocytic sites but are sometimes held at a short distance from sites marked by Sec3 and Exo70.

We examined the colocalization of Sec2GEF-mCherry-CUE or Sec2-mCherry with Myo2-GFP, a type V myosin protein that is recruited to secretory vesicles by Sec4-GTP (Jin *et al.*, 2011). At polarized sites they exhibited colocalization in both strains, but nonpolarized Sec2GEF-mCherry-CUE puncta displayed a lower degree of colocalization with Myo2-GFP (Figure 3C). In the case of Sro7, a SNARE regulator that binds to Sec4-GTP (Grosshans *et al.*, 2006a), even the polarized Sec2GEF-mCherry-CUE puncta displayed a low degree of Sro7-GFP colocalization and nonpolarized Sec2GEF-mCherry-CUE puncta were largely unlabeled by Sro7-GFP (Figure 3D). Together these results indicate that while Sec-2GEF-mCherry-CUE can recruit and activate Sec4, the efficiency of recruitment of downstream Sec4 effectors appears to be somewhat reduced relative to full-length Sec2, particularly at nonpolarized sites and particularly for Sro7. Successful recruitment of Myo2 would be expected to lead to the movement of structures along actin cables toward polarized sites. This explains why the Sec-2GEF-mCherry-CUE structures lacking Myo2-GFP are preferentially found at nonpolarized sites.

Sec9 is not a direct effector of Sec4. It is a tSNARE that binds to Sro7 and thereby acts downstream of Sec4 (Brennwald *et al.*, 1994; Lehman *et al.*, 1999; Grosshans *et al.*, 2006a). We coexpressed Sec-2GEF-mCherry-CUE or Sec2-mCherry and Sec9-GFP. Sec2-mCherry and Sec9-GFP display extensive colocalization at polarized sites. In contrast, Sec2GEF-mCherry-CUE puncta, either at polarized sites or at nonpolarized sites, were predominantly negative for Sec9-GFP colocalization (Supplemental Figure S4B). The low extent of colocalization could reflect inefficiency in the activation of SNARE function in response to Sec2GEF-mCherry-CUE, consistent with the analysis of vesicle tethering indicating an extended lifetime of tethered vesicles.

FIGURE 1: Sec2GEF-GFP-CUE and Sec2GEF-NeonGreen-CUE localize to polarized sites with reduced dynamics, and overexpression of Sec4 enhances the localization of Sec2GEF-GFP or Sec2GEF-GFP-CUE^{M419D} at polarized sites. (A) GFP images and DIC images overlaid with GFP images of representative cells grown to early log phase in SC medium at 25°C. The strains examined are *sec2*Δ containing an integrated plasmid expressing full-length Sec2-GFP, Sec2GEF-GFP, Sec2GEF-GFP-CUE, or Sec2GEF-GFP-CUE^{M419D} from the Adh1 promoter. Open arrowheads and arrows point to puncta localized at polarized sites including bud tip or bud neck and at nonpolarized sites, respectively. Bars, 5 μm. Sec2-GFP, Sec2GEF-GFP, Sec2GEF-GFP-CUE, or Sec2-GEF-GFP-CUE^{M419D} puncta localization at polarized or nonpolarized sites was quantified and is shown on the right panel. The error bars in the graph are the SD from three independent experiments. (B) Representative images of GFP-label, mCherry-Sec4, merged and overlay DIC with merged images in *SEC2GEF-GFP-CUE, SEC2GEF-GFP-CUE*M419D, *SEC2GEF-GFP*, or *SEC2-GFP* strains as indicated on the left panel. Bar, 5 μm. Open arrowheads and arrows point to GFP puncta localized at polarized sites and nonpolarized sites, respectively. The localization of Sec2GEF-GFP-CUE, Sec2GEF-GFP-CUE^{M419D}, Sec2GEF-GFP, and control Sec2-GFP at polarized sites in the absence or presence of overexpressed Sec4 was quantified and is shown on the right panel. Sec2-GFP is well localized at polarized sites, and Sec4 overexpression does not affect it. (C) Early log–phase cells expressing Sec2-NeonGreen or Sec2GEF-NeonGreen-CUE as the sole copy of Sec2 under the Adh1 promoter were analyzed by time-lapse fluorescence imaging for 90 s (see Supplemental Movies S1 and S2). The persistence time (in seconds) of identified vesicle puncta in wild-type *SEC2-NeonGreen* cells ($n = 26$) and mutant *SEC2GEF-NeonGreen-CUE* cells ($n = 29$) was determined as described in *Materials and Methods*. Because the acquisition time is a total of 90 s and more than 50% of the puncta tracked in *SEC2GEF-NeonGreen-CUE* cells persisted until the end of acquisition, we describe the vesicle dynamics using the percentage of vesicle puncta in various persistence time groups. (D) FRAP experiments showing the normalized fluorescence intensity in the entire small bud for tagged full-length Sec2-NeonGreen or Sec2GEF-NeonGreen-CUE (see Supplemental Movies S3 and S4). The original fluorescence intensity (time = 0 s) is normalized to 100% before photobleaching, and during the time-lapse acquisition the cells selected are photobleached (time = 2 s, marked by the arrow). Plotted points represent the mean value of five replicate samples each. The photobleach and FRAP experimental details are described in *Materials and Methods*. (E) Still frames of a typical vesicle-tracking experiment after FRAP in wild-type *SEC2-NeonGreen* or *SEC2GEF-NeonGreen-CUE* cells. An inverted monochrome maximum projection is shown for clarity. Arrows point to Sec2-NeonGreen or Sec2GEF-NeonGreen-CUE puncta tethered to the membrane (see also Supplemental Movies S5 and S6). Bar, 2 μm. Kymograph used to measure the persistence time (likely from tethering to fusion) of the vesicle puncta shown by the arrows in the left panel. The quantification was done in wild-type *SEC2-NeonGreen* cells ($n = 42$) and mutant *SEC2GEF-NeonGreen-CUE* cells ($n = 56$), and the percentage of vesicle puncta in various persistence time groups are shown in the right panel.

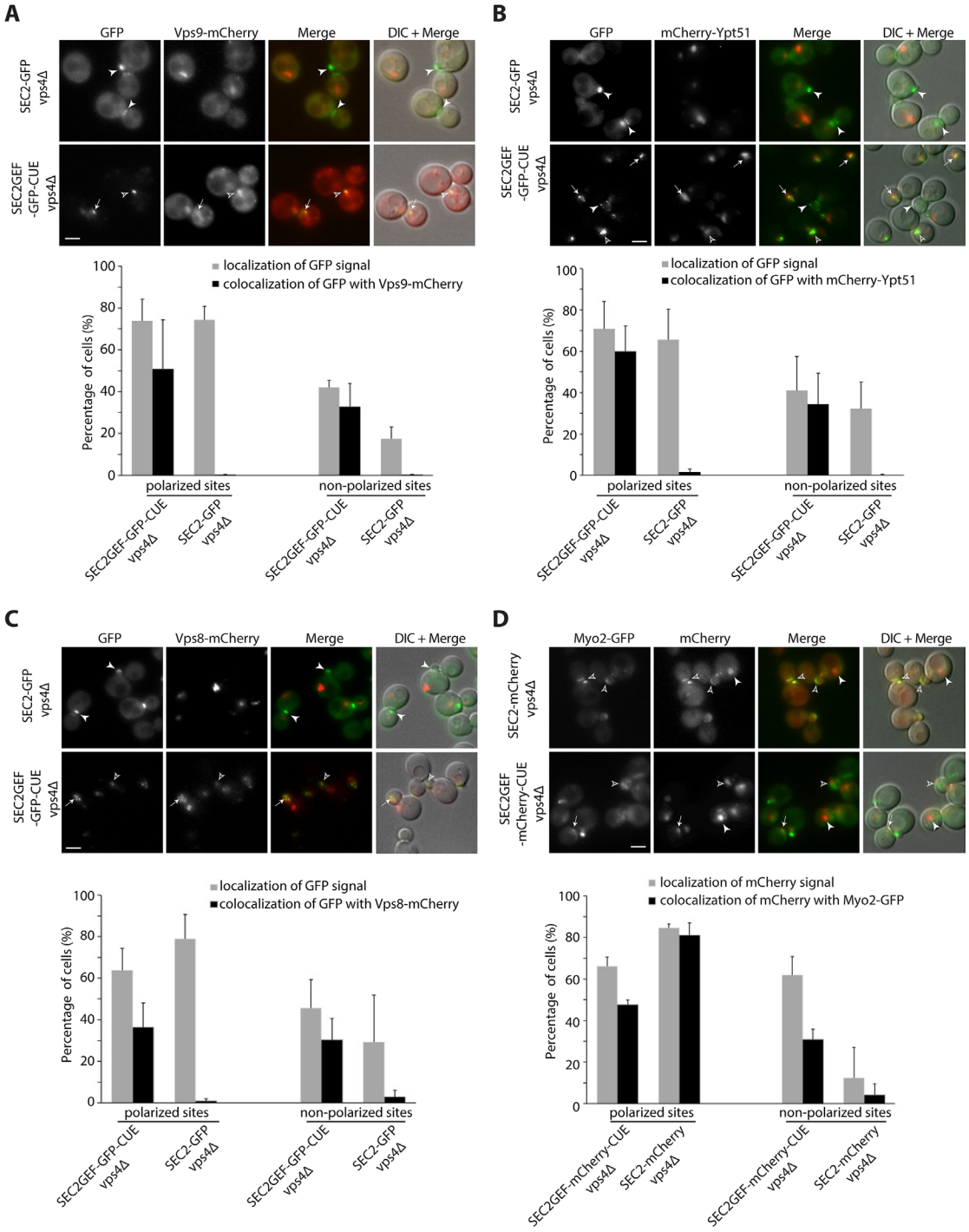

FIGURE 2: Localization of Sec2GEF-GFP-CUE (Sec2GEF-mCherry-CUE) or Sec2-GFP (Sec2-mCherry) and their colocalization with distinct Rabs or Rab effectors on the secretory and endocytic pathways in *vps4*Δ strains. (A–C) Live-cell fluorescence microscopy of *SEC2-GFP* and *SEC2GEF-GFP-CUE* strains expressing Vps9-mCherry (A), mCherry-Ypt51 (B), or Vps8-mCherry (C) is shown on top panels. The quantification of Sec2-GFP and Sec2GEF-GFP-CUE localization at polarized or nonpolarized sites and their colocalization with the indicated mCherry-tagged proteins are shown in the bottom panels. Open arrowheads and arrows indicate, respectively, polarized sites and nonpolarized sites at which GFP colocalizes with mCherry-tagged proteins, while closed arrowheads point to GFP puncta that are not colocalized with the other protein examined. In all quantitation graphs the error bars represent the SD from three independent experiments. Scale bar, 5 μm. (D) Localization of Sec2GEF-mCherry-CUE or Sec2-mCherry and their colocalization with Myo2-GFP in *vps4*Δ strains. Top panel shows representative GFP fluorescence, mCherry fluorescence, merged, and DIC overlaid with merged images. The quantification of Sec2-mCherry and Sec2GEF-mCherry-CUE localization at polarized or nonpolarized sites and their colocalization with Myo2-GFP proteins are shown in the bottom panel. Open arrowheads and arrows, respectively, indicate polarized sites and nonpolarized sites at which mCherry colocalizes with Myo2-GFP, while closed arrowheads point to mCherry puncta that are not colocalized with Myo2-GFP. In all quantitation graphs the error bars represent the SD from three independent experiments. Scale bar, 5 μm.

Sec2GEF-GFP-CUE expression leads to minor dominant negative growth defects and synthetic negative interactions with a subset of secretory and endocytic mutants

We first evaluated the function of the various Sec2 constructs in a *sec2* null background. When expressed from the *SEC2* promoter or from the *ADH1* promoter integrated at the *URA3* locus, both Sec2GEF-GFP-CUE and Sec2GEF-GFP were able to complement the lethality of a *SEC2* deletion (Figure 4A). Growth was modestly impaired at 37°C in cells expressing Sec2GEF-GFP-CUE from the *SEC2* promoter at the *URA3* locus. A mutation within the CUE domain (M419D) that blocks interaction with ubiquitin moieties restored normal growth. A modest growth defect was observed at 25°C when Sec2GEF-GFP-CUE was expressed from the stronger *Gal1* promoter in either a *sec2*Δ or a *SEC2* background (Figure 4B). This minor, dominant negative effect was blocked by the M419D mutation in the CUE domain. In total, the results indicate surprisingly mild effects on growth of fusing the Sec2GEF to the CUE domain. Nonetheless, the effects observed were at least partially dominant and could be negated by blocking the interaction of the CUE domain with ubiquitin. The *vps4*Δ mutation results in slow growth at 37°C; however, expression of Sec2GEF-GFP-CUE in the *vps4*Δ background does not cause any additional growth inhibition (Figure 4C). The GFP tag appears to confer stability of the fusion proteins because severalfold-higher levels of Sec2-GFP were detected relative to unfused Sec2 (Elkind *et al.*, 2000) and different tagged versions of Sec2 or Sec2GEF-CUE constructs exhibit similar expression levels (Supplemental Figure S5A). This is indeed the case because a Sec2GEF construct lacking a GFP tag expressed from the *SEC2* promoter integrated at the *URA3* locus was unable to complement the lethality of a *SEC2* deletion (Supplemental Figure S5B). Sec2GEF expressed from the *SEC2* promoter did not exhibit a detectable level of protein while Sec2GEF-GFP expressed from a parallel construct was readily detected (Supplemental Figure S5C).

Genetic interactions can reveal a partial loss of function and can be informative regarding the site of action of different mutant alleles. We crossed a strain expressing Sec2GEF-GFP-CUE to a variety of different secretory mutants (Table 1). Synthetic negative interactions were observed with a subset of the strains tested, including certain mutations in the exocyst complex (*sec5-24*, *sec8-9*, and *sec10-2*, but not *sec6-4*), a tSNARE (*sec9-4*), a SNARE regulator (*sro7*Δ, but not *sec1-1*), and Rab GDI (*sec19-1*). No interaction was seen with the endoplasmic reticulum (ER) mutant *sec12-4*. These results are consistent with an inhibitory effect of Sec2GEF-GFP-CUE on the final stage of the secretory pathway. This effect is not strongly growth limiting on its own but becomes more apparent in a sensitized genetic background.

We also tested the synthetic growth phenotype of Sec2GEF-GFP-CUE with several different endocytic mutants (Table 1). Synthetic negative interactions were observed with a deletion of the endocytic Rab, *ypt51*Δ, or its GEF, *vps9*Δ, but no interaction was seen with two endocytic cargo receptor mutants, *syp1*Δ and *ede1*Δ.

Sec2GEF-GFP-CUE expression delays the Snc1 cycle at a late stage of the secretory pathway and leads to the accumulation of secretory vesicles

The exocytic vSNARE, Snc1, cycles continuously from secretory vesicles to the plasma membrane of the bud and then into endocytic vesicles and the Golgi before it is repackaged into a new round of secretory vesicles (Lewis *et al.*, 2000). A slowing of any stage of this cycle leads to a localized buildup of Snc1, even if it is not rate limiting for growth. We coexpressed GFP-Snc1 with Sec2GEF-mCherry-CUE or Sec2-mCherry. In cells expressing Sec2-mCherry, as in wild-type cells, GFP-Snc1 was found predominantly at the plasma membrane, preferentially enriched in the bud. In addition, several internal puncta representing endocytic compartments and Golgi were observed in most cells (Figure 5A). In 45% of cells expressing Sec2GEF-mCherry-CUE, a prominent patch of GFP-Snc1 was seen, often in small buds or near the neck of large-budded cells (Figure 5A). The formation of a patch of GFP-Snc1 near sites of polarized growth is consistent with a delay in the Snc1 cycle at a late stage of the secretory pathway.

Thin-section electron microscopy (EM) analysis revealed the presence of clusters of 80-nm-diameter vesicles in cells expressing Sec2GEF-GFP-CUE (Figure 5B). These clusters were observed in the bud as well as in the mother cell, consistent with the appearance of the Sec2GEF-GFP-CUE puncta by fluorescence microscopy. Cells expressing Sec2-GFP exhibited isolated 80-nm-diameter vesicles, which were typically at the bud tip or near the neck. Quantitative analysis demonstrated approximately twice as many vesicles per section in cells expressing Sec2GEF-GFP-CUE relative to cells expressing Sec2-GFP (Figure 5C).

Despite the accumulation of vesicles, a direct assay of the export of the cell wall glucanase Bgl2 did not reveal a significant intracellular accumulation (Supplemental Figure S6). To explore the possibility of a subtle defect on the secretory pathway, we analyzed the effects of Sec2GEF-GFP-CUE expression in a sensitized *sro7*Δ background. The *sro7*Δ single mutant exhibited a minor intracellular accumulation of Bgl2; the *sro7*Δ *SEC2GEF-GFP-CUE* double mutant had a much stronger defect (Supplemental Figure S7A). An intermediate result was seen in the *sro7*Δ *SEC2-GFP* control. Similarly, thin-section EM showed a much greater accumulation of secretory vesicles in the *sro7*Δ *SEC2GEF-GFP-CUE* double mutant than in the *sro7*Δ single mutant (Supplemental Figure S7, B and C). In total, the results support the conclusion that Sec2GEF-GFP-CUE expression leads to a minor defect at the final stage of the secretory pathway that can be exacerbated in a sensitized background.

Endocytosis of Mup1-GFP is slowed in Sec2GEF-mCherry-CUE–expressing cells with a transient association of Sec2GEF-mCherry-CUE with internalized Mup1-GFP

The engineered recruitment of exocytic components onto endocytic membranes raised the possibility of impaired endocytosis. We assessed the rate of endocytosis using the methionine permease, Mup1. In the absence of methionine in the growth medium, this permease resides in the plasma membrane; however, within minutes of methionine addition, Mup1 is ubiquitinated, internalized into endosomes, and delivered to the vacuole for degradation (Guiney *et al.*, 2016). We followed Mup1-GFP through a time course from 3 to 63 min after addition of 20 µg/ml methionine. In cells expressing either Sec2GEF-mCherry-CUE or Sec2-mCherry, Mup1-GFP was observed exclusively at the plasma membrane before methionine addition and following methionine addition, it was delivered from the plasma membrane to the vacuole (Figure 6A and Supplemental Figure S8). Rectangular regions of the plasma membrane were selected for quantitation of Mup1-GFP fluorescence intensity. The rate of clearance from the plasma membrane was significantly slowed in Sec2GEF-mCherry-CUE cells relative to Sec2-mCherry cells (Figure 6B; Supplemental Movies S7 and S8), as was delivery to the vacuole (Supplemental Figure S8B). Transient colocalization of Mup1-GFP with Sec2GEF-mCherry-CUE was observed. As shown by still-frame images in Figure 6C, the two signals either colocalized completely (indicated by open arrowheads) or partially overlapped with each other (indicated by closed arrowheads), suggesting that these two

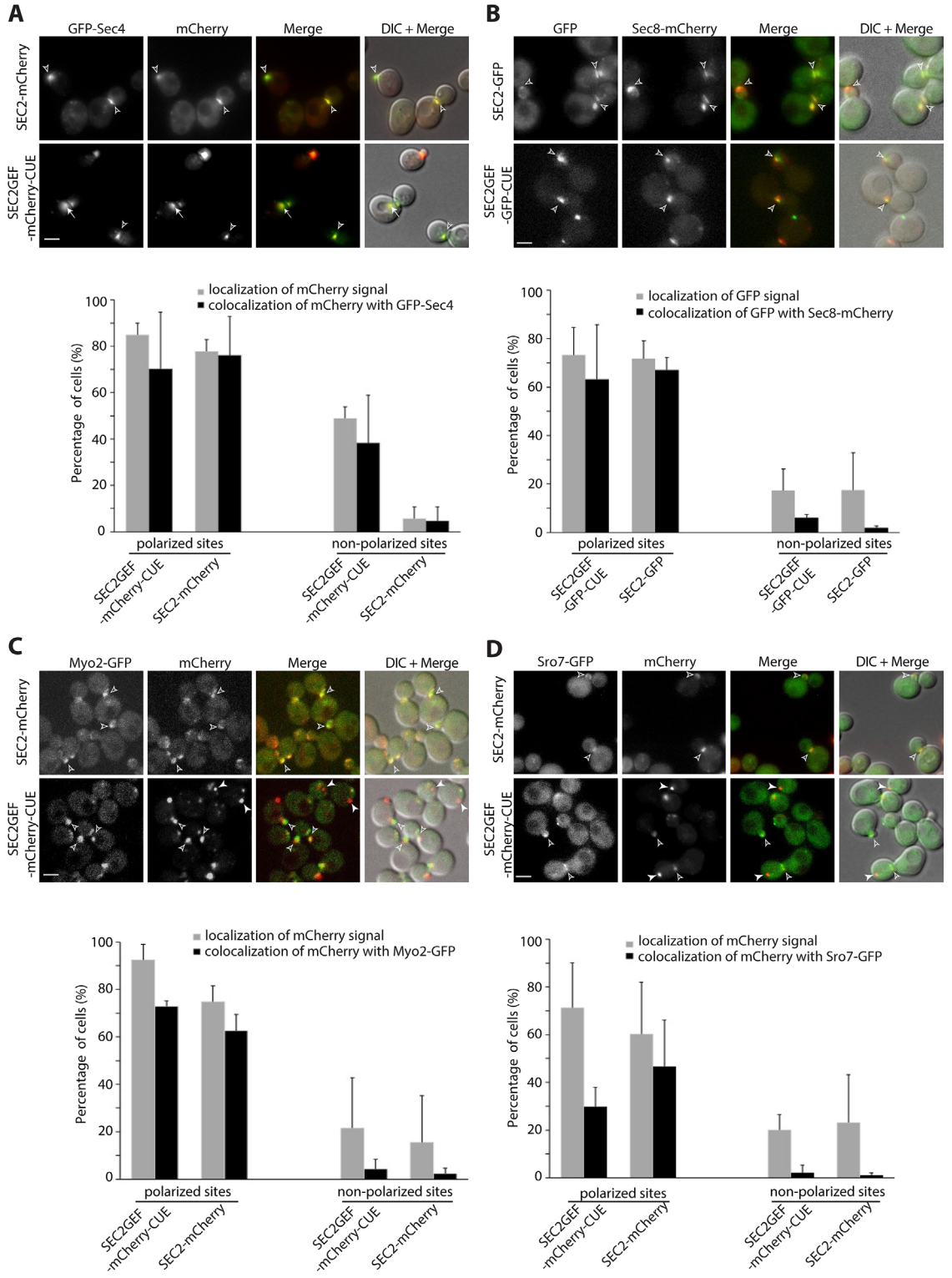

FIGURE 3: Sec2GEF-GFP-CUE recruits Sec4 to both polarized and nonpolarized sites, but preferentially recruits Sec4 effectors to polarized sites. From panel A to panel D, representative images of the mCherry-fluorescence channel, GFP channel, merged image, or overlay DIC with merged images of the indicated cells are shown in the top panels and quantification of the results in the bottom panels. The error bars represent the SD from three independent experiments. Scale bars, 5 μm. (A) Colocalization results of GFP-Sec4 with Sec2-mCherry or Sec2GEF-mCherry-CUE. Open arrowheads point to colocalized GFP-Sec4 with Sec2-mCherry or Sec2GEF-mCherry-CUE at polarized sites, bud tip in small buds or bud neck in large buds, respectively. Arrows point to colocalized GFP-Sec4 with Sec2GEF-mCherry-CUE at nonpolarized sites. There is rarely colocalization of GFP-Sec4 with Sec2-mCherry at nonpolarized sites. (B) Colocalization results of exocyst Sec8-mCherry with Sec2-GFP or Sec2GEF-GFP-CUE. Open arrowheads point to colocalized Sec8-mCherry with Sec2-GFP or Sec2GEF-GFP-CUE at polarized sites. At nonpolarized sites there is a low

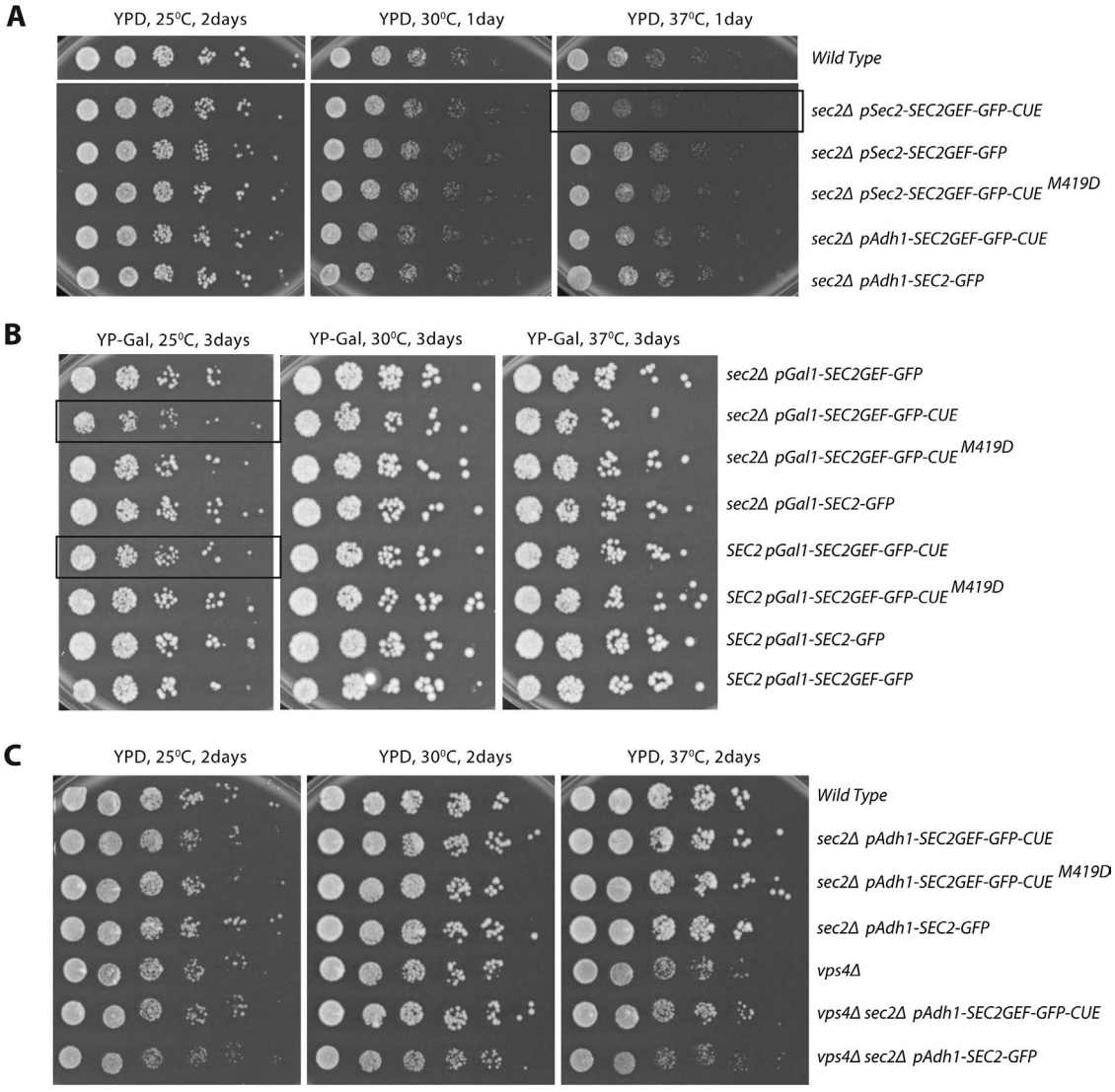

FIGURE 4: Growth phenotypes of *SEC2GEF-GFP-CUE* mutants expressed from different promoters. (A) Serial dilutions of the overnight cultures from the indicated strains were plated on YPD plates and grown for 1 or 2 d at different temperatures as shown. Constructs are expressed from the Adh1 promoter or the Sec2 promoter as indicated. (B) Serial dilutions of the overnight cultures from the indicated strains were plated on YP galactose plates to induce protein expression under the Gal1 promoter and grown for 3 d at different temperatures as shown. Constructs either are in a *sec2*Δ background or are coexpressed with endogenous Sec2 as indicated. Strains exhibiting mild growth defects are framed. (C) Serial dilutions of the overnight cultures from the indicated strains were plated on YPD plates and grown for 2 d at different temperatures as shown. Constructs are in a *vps4*Δ or endogenous *VPS4* background.

proteins might transiently exist within the same compartment rather than directly binding to each other.

DISCUSSION

We have explored the effects of fusing the catalytic domain of an exocytic Rab GEF onto a CUE endocytic localization domain. Our expectation was that this construct would be recruited to endocytic membranes, which would in turn lead to the ectopic recruitment of Sec4 and its effectors. If Rabs specify the direction of vesicular transport, this could potentially lead to fusion of endocytic compartments with the plasma membrane rather than normal passage along the endocytic pathway. We observed localization of the Sec2GEF-GFP-CUE fusion protein to prominent cytoplasmic puncta that was strongly dependent on the ubiquitin-binding activity of the CUE domain. Electron microscopy showed that these puncta represent aberrant clusters of 80-nm vesicles. This implies that the fusion

percentage of colocalization of Sec8-mCherry with Sec2GEF-GFP-CUE and barely any with Sec2-GFP. (C) Colocalization of Myo2-GFP with Sec2-mCherry or Sec2GEF-mCherry-CUE at polarized sites (open arrowheads). There is rarely colocalization of Myo2-GFP with Sec2-mCherry or Sec2GEF-mCherry-CUE at nonpolarized sites (closed arrowheads). (D) Sro7-GFP is well colocalized with Sec2-mCherry and partially colocalized with Sec2GEF-mCherry-CUE at polarized sites (open arrowheads), but there is barely colocalization of Sro7-GFP with either Sec2GEF-mCherry-CUE or Sec2-mCherry at nonpolarized sites. Closed arrowheads point to noncolocalized Sro7-GFP with Sec2GEF-mCherry-CUE.

Mutant strain	Growth at 25°C	Growth at 37°C	Growth at 16°C
sec1-1 SEC2-GFP	+++	–	+++
sec1-1 SEC2GEF-GFP-CUE	+++	–	+++
sec5-24 SEC2-GFP	+++	–	+++
sec5-24 SEC2GEF-GFP-CUE	+	–	±
sec6-4 SEC2-GFP	+++	–	+++
sec6-4 SEC2GEF-GFP-CUE	+++	–	+++
sec8-9 SEC2-GFP	+++	–	+++
sec8-9 SEC2GEF-GFP-CUE	+	–	–
sec9-4 SEC2-GFP	+++	–	+++
sec9-4 SEC2GEF-GFP-CUE	+	–	++
sec10-2 SEC2-GFP	+++	–	+++
sec10-2 SEC2GEF-GFP-CUE	+	–	++
sec12-4 SEC2-GFP	+++	–	+++
sec12-4 SEC2GEF-GFP-CUE	++	–	+++
sec19-1 SEC2-GFP	+++	–	+++
sec19-1 SEC2GEF-GFP-CUE	++	–	++
sro7Δ SEC2-GFP	+++	+++	+++
sro7Δ SEC2GEF-GFP-CUE	+++	+++	++
ede1Δ SEC2-GFP	+++	+++	+++
ede1Δ SEC2GEF-GFP-CUE	+++	+++	+++
syp1Δ SEC2-GFP	+++	++	+++
syp1Δ SEC2GEF-GFP-CUE	+++	++	+++
vps9Δ SEC2-GFP	+++	+++	+++
vps9Δ SEC2GEF-GFP-CUE	+++	++	+++
ypt51Δ SEC2-GFP	+++	+++	+++
ypt51Δ SEC2GEF-GFP-CUE	+++	++	+++

±, very sick; +, obvious slow growth; ++, a little slower than wild-type growth; +++, wild type–like growth.

TABLE 1: Synthetic growth defects of secretory mutant or endocytic mutant strains when combined with *SEC2GEF-GFP-CUE*.

protein associates with vesicles containing ubiquitinated endocytic cargo, and this was confirmed by the observation of transient colocalization with internalized Mup1. In a *vps4Δ* mutant, in which turnover of ubiquitinated endocytosed proteins is blocked, we observed increased colocalization of Sec2GEF-GFP-CUE with endogenous Vps9, its target Rab, Ypt51, a late endosomal marker, Vps8, and a probe for PI3P. As predicted, this triggers recruitment of Sec4 and at least some of its downstream effectors, including the myosin motor, Myo2, resulting in their delivery to polarized sites. Thus, the data suggest that we had in fact directed an exocytic Rab and exocytic machinery onto endocytic membranes, as intended. Nonetheless, the phenotypic effects we observed were surprisingly mild; cell growth and protein secretion were nearly normal. These results imply that Golgi-derived secretory vesicles carrying exocytic cargo were still able to successfully engage the Myo2 myosin motor, the exocyst vesicle tether, and the SNARE-dependent fusion machinery, despite the substantial misdirection of Sec4 to endocytic membranes.

A clue to one possible basis for the surprising resilience of the exocytic pathway came from our analysis of the Sec2GEF-GFP construct that we used as a control. This fusion protein, lacking all known Sec2 localization domains, was nonetheless able to localize to sites of polarized growth in a small fraction of the cells. Importantly, this residual localization increased upon overexpression of Sec4, suggesting that the Sec2GEF-GFP construct can be recruited to vesicles by Sec4. A downstream effector with an independent localization mechanism, such as the exocyst (Shen *et al.*, 2013), might promote the vesicle association of Sec4 by blocking GDI-mediated extraction, as has been suggested for several other Rabs (Aivazian *et al.*, 2006; Cabrera and Ungermann, 2013). While this mechanism is inefficient, as demonstrated by the low extent of polarized Sec2GEF-GFP localization, it is apparently sufficient to maintain secretory function and normal growth when aided by the increased stability resulting from fusion to GFP. In the case of the Sec2GEF-GFP-CUE construct, this secretory vesicle localization pathway would act in competition with the CUE domain–dependent endocytic localization pathway, to promote secretion and viability. Pertinent to this possibility, we found that deletion of *VPS4* increases recruitment of Sec2GEF-GFP-CUE to enlarged endosomes but does not impair growth.

Another possible explanation for the mild effects of Sec2GEF-GFP-CUE expression is suggested by the proposal that the TGN serves the role of the early endosome in yeast (Day *et al.*, 2018). By this proposal, endocytic vesicles fuse with the TGN and then vesicles derived from the TGN carrying endocytic cargo are directed to the late endosome. Vps9 is thought to be initially recruited to the TGN and then incorporated into these vesicles destined for the late endosome (Nagano *et al.*, 2019). If Sec2GEF-GFP-CUE were similarly recruited to the TGN by ubiquitinated endocytic proteins, it could potentially help carry secretory cargo proteins destined for the cell surface from the TGN, mimicking the normal exocytic route. This possibility would also explain the observed delay in the delivery of endocytic proteins to the vacuole in Sec2GEF-GFP-CUE cells, as some fraction would be recycled from the TGN back to the cell surface instead of to the late endosome. While we observed no colocalization of Sec2GEF-GFP-CUE with a TGN marker, it is hard to exclude a transient association. It is important to note that our construct contained only the CUE domain of Vps9, while full-length Vps9 is thought to also rely on an interaction with Arf1 for TGN recruitment. It is not clear how the lack of an Arf1 binding domain might affect the site of recruitment of Sec2GEF-GFP-CUE.

The association of Sec2GEF-GFP-CUE with endocytic vesicles was not completely benign. We observed weak, dominant negative effects on growth. These effects were relieved by a mutation within the CUE domain that blocks ubiquitin binding, implying that the growth inhibitory mechanism of Sec2GEF-GFP-CUE requires its association with endocytic cargo. Furthermore, delivery of Mup1-GFP to the vacuole was slowed in Sec2GEF-GFP-CUE cells and synthetic negative effects on growth were observed in combination with *vps9Δ* or *ypt51Δ*. The prominent Sec2GEF-GFP-CUE puncta were largely static and did not appear to fuse with the plasma membrane at an appreciable rate; however, as these bright puncta represent vesicle clusters, individual vesicles may go on to fuse with the plasma membrane even as the cluster appears to be static. While most of these puncta acquired Sec4 and its effectors, including the exocyst and Myo2, others failed to acquire Myo2 and were therefore not delivered to polarized sites. Many also failed to acquire the effector Sro7 and appeared to be unable to efficiently assemble a SNARE complex with the tSNARE Sec9 despite the presence of the vSNARE Snc1. Although these compartments carried both Sec4 and the Snc1 vSNARE, they were delayed in fusion with the plasma membrane, implying the requirement for an additional component for fusion competence. We speculate that this component could be the

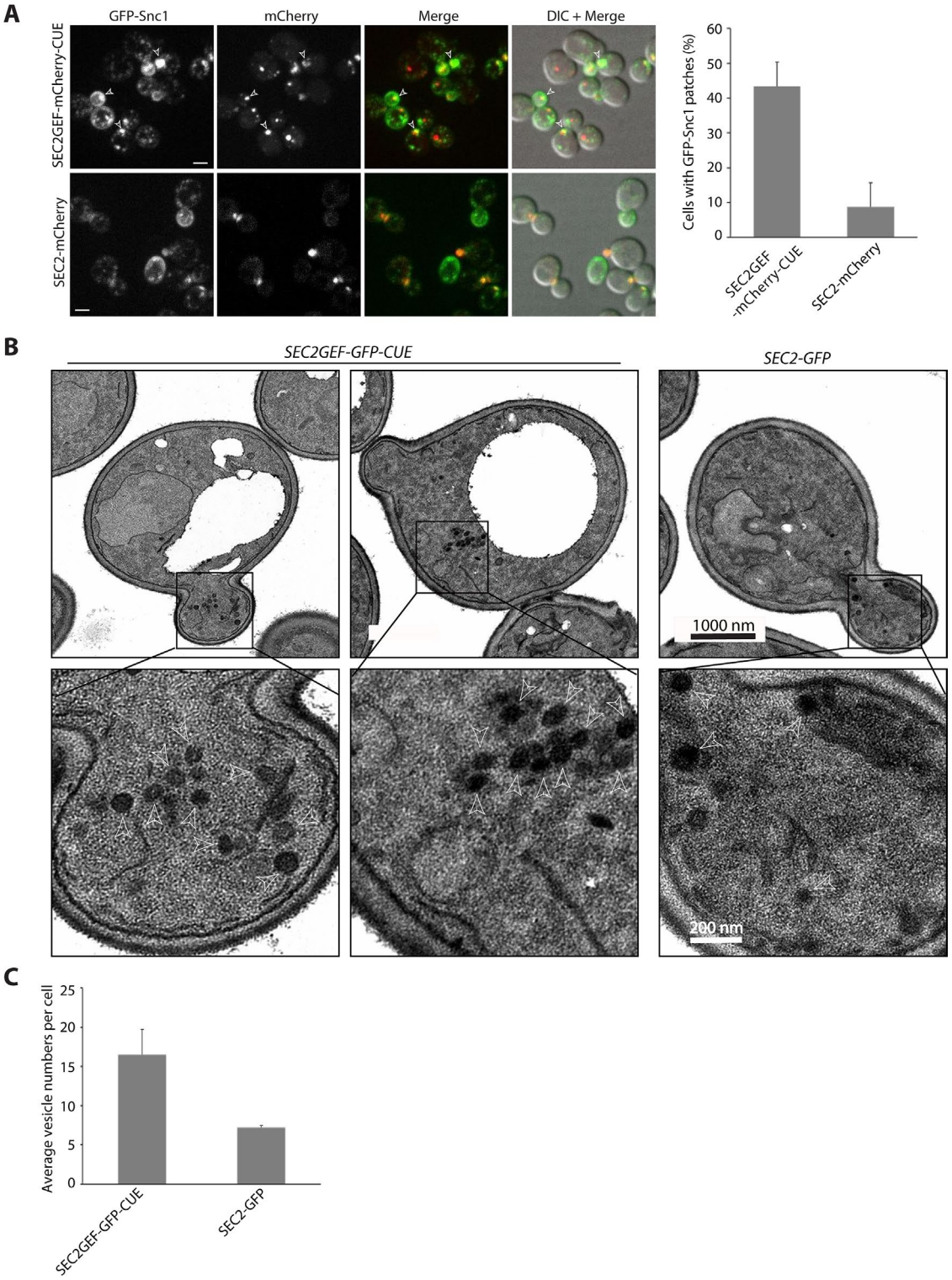

FIGURE 5: The *SEC2GEF-CUE* mutant has mild secretion defects shown by GFP-Snc1 localization and EM. (A) Left panel shows representative fluorescence images of GFP-Snc1, the mCherry channel, a merge of the two channels, and overlay DIC with merged images in *SEC2-mCherry* or *SEC2GEF-mCherry-CUE* cells grown to early log phase in SC medium at 25°C. Open arrowheads point to accumulated GFP-Snc1 patches. Bars, 5 μm. The percentage of cells that contained GFP-Snc1 patches in the indicated strains was quantified (right panel). The error bars represent the SD from three independent experiments. (B) Thin-section EM images from the strains indicated were prepared as described in *Materials and Methods*. The cells were fixed in potassium permanganate. Representative images at 10,000× magnification are shown on the top panels. The expanded boxed regions from the top panels are shown on the bottom panels. Arrowheads indicate vesicles, and scale bars are indicated. (C) Quantitation of secretory vesicles per cell. More than 100 cells were analyzed for each strain.

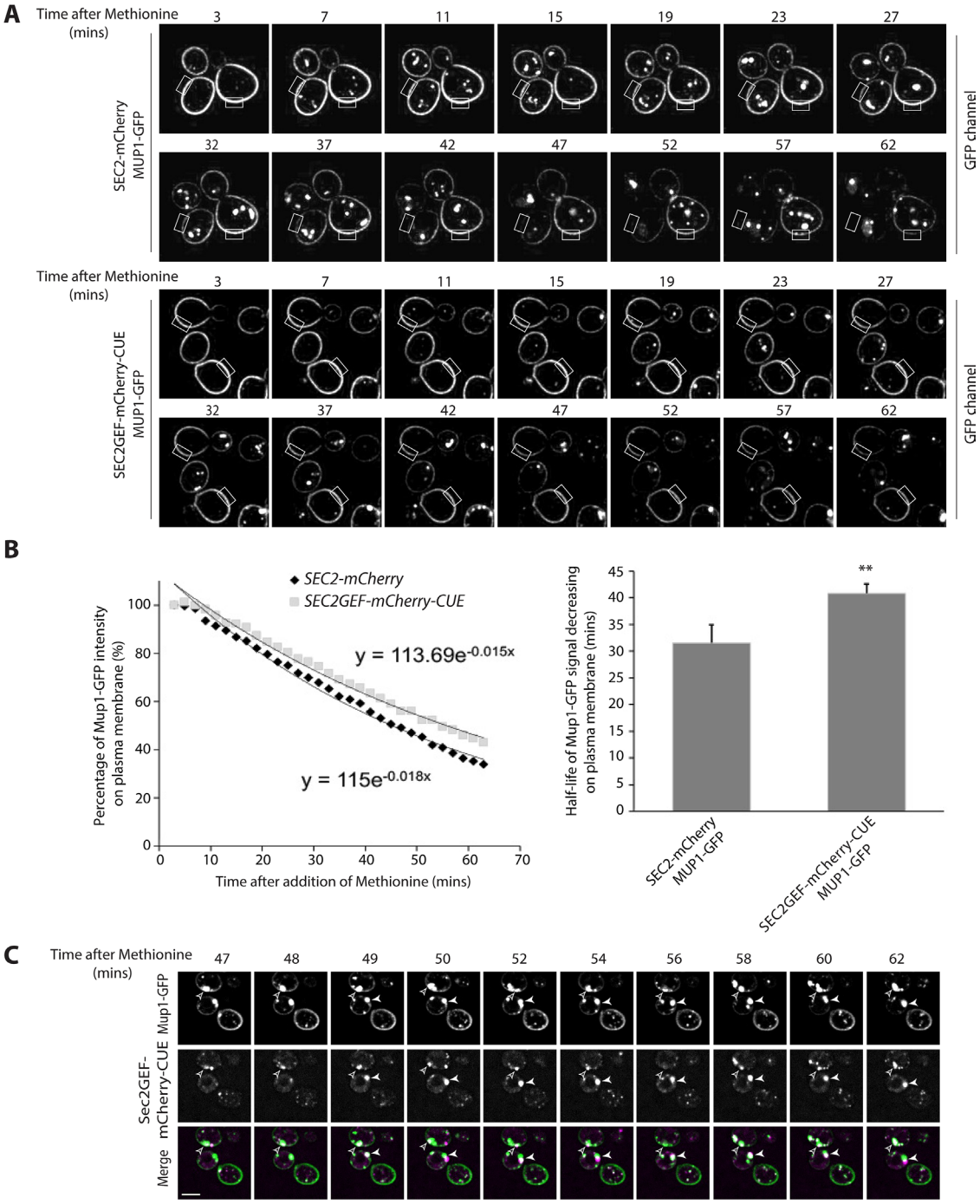

FIGURE 6: Endocytosis is slow in *SEC2GEF-mCherry-CUE* cells, and following internalization Mup1-GFP transiently colocalizes with Sec2GEF-mCherry-CUE. (A) Live-cell fluorescence microscopy of Mup1-GFP expressed from the chromosomal locus after the addition of 20 μg/ml methionine to stimulate internalization of Mup1-GFP from the plasma membrane and transport to the vacuole lumen in *SEC2-mCherry* (top panel) or *SEC2GEF-mCherry-CUE* (bottom panel) cells (also see Supplemental Movies S7 and S8). Representative images at the indicated time point are displayed and fluorescence intensity for the rectangle selection area used for quantitation. (B) Relative fluorescence intensity of Mup1-GFP at the plasma membrane was quantified and is plotted over time (left panel). Best-fit curves represent a single-exponential decay with one rate of loss from the plasma membrane. The half-times of Mup1-GFP signal decrease on the plasma membrane were 31.5 ± 3.4 s (*SEC2-mCherry*, $n = 7$) and 40.8 ± 1.7 s (*SEC2GEF-mCherry-CUE*, $n = 7$) as shown on the right panel. **, $P < 0.01$. (C) Still frames of representative cells during Mup1-GFP endocytosis at the indicated time points following the addition of 20 μg/ml methionine in the *SEC2GEF-mCherry-CUE* strain. Open and closed arrowheads indicate concentrated Mup1-GFP puncta adjacent to the vacuole at which Sec2GEF-mCherry-CUE completely colocalizes or partially overlaps with it. Bar, 5 μm.

phosphoinositide PI(4)P. This lipid is made in the TGN and incorporated into secretory vesicles but then depleted during vesicle maturation (Walch-Solimena and Novick, 1999; Mizuno-Yamasaki *et al.*, 2010; Ling *et al.*, 2014). While PI(4)P is known to promote Sec2 recruitment (Mizuno-Yamasaki *et al.*, 2010), it might have additional functions related to secretory vesicle function. Endocytic vesicles, in contrast, form PI(3)P, which acts to promote the formation of late endosomes (Peterson *et al.*, 1999). We observed significant colocalization of Sec2-GFP-CUE with a PI3P probe in *vps4*Δ cells.

In total, our results indicate that the directionality of vesicular transport cannot be reduced to simply the presence of a particular Rab but probably involves the interplay between the Rab, its effectors, and other vesicular components.

MATERIALS AND METHODS

Plasmid and yeast strain construction

The yeast strains and plasmids used in this study are listed in Supplemental Tables SI and SII. To generate the overexpression CEN vector NRB1680 (*pGal1-SEC2GEF-GFP-CUE*), Vps9-CUE (aa 408–451) was PCR amplified and by recombination inserted into NRB996 (*pGal-SEC2GEF-GFP, CEN*). Site-directed mutagenesis PCR was used to mutate the M419 codon to aspartic acid in the CUE domain to make vector NRB1681 (*pGal1-SEC2GEF-GFP-CUE*M419D). To generate the HemiZap vectors NRB1682, NRB1683, NRB1684, and NRB1685, fragments encoding Sec2GEF-GFP, Sec2GEF-GFP-CUE, Sec2GEF-GFP-CUE^{M419D}, and full-length Sec2-GFP were PCR amplified from NRB996, NRB1680, NRB1681, and NRB994 and then inserted into a *Xba*I/*Sal*I double-digested pRS306-ADH1t vector. NRB994 and NRB996 were made as described in Elkind *et al.* (2000). For mCherry- or NeonGreen-tagged versions of the Sec2 allele, fragments encoding mCherry or NeonGreen were amplified from template NRB1347 (*pJC1-pADH1-mCherry-SEC4*) or NHB0845 (*pFA6a-NeonGreen-His5*, kindly provided by Nan Hao at the University of California, San DiegoU) and swapped with the GFP tag in NRB1682, NRB1683, and NRB1685 by Gap repair recombination to generate plasmids NRB1686, NRB1687, NRB1688 or NRB1689, NRB1690. Similar approaches were used to generate Sec2 constructs expressed from the *SEC2* promoter. The SEC2 5′-noncoding sequence upstream of its open reading frame (ORF; 770 base pairs) was amplified and switched with the *ADH1* promoter in NRB1682, NRB1683, and NRB1684 by Gap repair to generate NRB1691, NRB1692, and NRB1693 constructs. The SEC2 5′-noncoding sequence upstream of its ORF (770 base pairs) and the first 480 nucleotide (nt) coding sequence were amplified and subcloned into the *Sac*I/*Xho*I cut plasmid NRB1691 to generate NRB1703. Similarly, The SEC2 5′-noncoding sequence upstream of its ORF (770 base pairs) and the first 786 nt coding sequence were amplified and subcloned into the *Sac*I/*Afl*II cut plasmid NRB1685 to generate NRB1704.

Because SEC2 is essential, it was necessary to delete the genomic copy of SEC2 in the diploid strain NY1523. NY3374 (*MAT*α*/a, SEC2/sec2*Δ*::his5*$^{+}$) was generated by replacing one copy of the *SEC2* coding sequence with the *Schizosaccharomyces pombe his5*$^{+}$ gene module using the PCR-mediated gene deletion method (Longtine *et al.*, 1998). To construct strains expressing various *sec2* alleles as the sole copy in yeast, HemiZAP *sec2*–expressing plasmids were digested with a unique enzyme (see Supplemental Table SII) and introduced into yeast diploid cells (NY3374) at the URA3 locus by homologous recombination. After sporulation and tetrad dissection, the spores were analyzed and we selected representatives that carried only the mutant *sec2* allele with a C-terminal tag. For *GAL1* promoter–driven overexpression constructs of *SEC2*, CEN plasmids NRB996, NRB1680, NRB1681, and NRB994 were directly transformed into wild-type yeast cells, NY1210, and grown in SC-Ura3 with 2% galactose condition to induce *sec2* allele overexpression in the presence of wild-type untagged *SEC2*. Alternatively, these CEN plasmids were transformed into a diploid yeast strain (NY3374) and after sporulation and tetrad dissection the haploids with only one copy of the mutant *sec2* allele on a plasmid were selected.

Two *SEC4* integration plasmids were used. One is tagged with mCherry at its N-terminus and overexpressed from the strong *ADH1* promoter (NRB1347). Another one is tagged with GFP at its N-terminus and expressed under its own promoter (NRB1694). It was subcloned from NRB1312 (*pRS306-pSec4-GFP-SEC4-tSEC4*) into NRB1695 (*pRS305-myo2-GFP*) using *Xho*I/*Sac*I. NRB1347 was linearized with *Afl*II to integrate into the *LEU2* locus, while NRB1694 was linearized with *Sph*I to integrate into the *SEC4* locus. To generate the Hemizap *pRS305-myo2-GFP* vector (NRB1695), a C-terminal fragment of *MYO2* (3189–4722 base pairs) was amplified by PCR from gDNA and subcloned into the *pRS305-GFP* plasmid with *Xho*I and *Sac*II. The plasmid was linearized using *Stu*I and integrated into the *MYO2* locus. Similar approaches were used to generate *EXO70*, *SEC3*, *SEC8*, *SEC15*, and *VPS9* HemiZAP constructs (NRB1565, NRB1329, NRB1460, NRB1697, and NRB1696).

To generate the Hemizap *GFP-SEC9-LEU2* vector (NRB1698), a fragment encoding the *SEC9* promoter 1026 base pairs, the GFP module 738 base pairs, and the *SEC9* N-terminal 705-base-pair ORF were amplified by PCR from genomic DNA (gDNA) or a common plasmid and sequentially subcloned into plasmid NRB1631 using *Xho*I/*Xma*I, *Xma*I/*Xba*I, and *Xba*I/*Pst*I to replace the sequence of *pSec5-Tos2(2-74)-Sec5N*. The final plasmid was linearized with *Bgl*II and transformed into yeast at the *SEC9* locus. To generate the mCherry-Ypt51 integration vector (NRB1700), the *YPT51* ORF sequence was amplified by PCR from gDNA and subcloned into NRB1347 to replace the *SEC4* sequence using *Bam*HI/*Sal*I. This plasmid was linearized using *Afl*II and integrated into the *LEU2* locus. To switch the auxotrophic marker of the Vps8-mCherry integration vector (NRB1699), the *VPS8-6xmCherry* sequence was excised from *YIplac211-VPS8-6xmCherry* (generous gift from B. Glick) (Losev *et al.*, 2006) and subcloned into a pJC1 vector by *Hin*dIII/*Sac*I. This plasmid was linearized using *Bcl*I and integrated into the *VPS8* locus. Similarly the *SEC7-6xdsRed* sequence was excised from NRB1338 (*YIplac204-SEC7-6xdsRed)* (Losev *et al.*, 2006) and subcloned into the pJC1 vector by *BstAP*I/*Pvu*I. This plasmid (NRB1702) was linearized using *Age*I and integrated into the *LEU2* locus. To switch the auxotrophic marker of the mRFP-FYVE(EEA1) integration vector (NRB1706), the *mRFP-FYVE(EEA1)* sequence was excised from *pRS416-mRFP-FYVE(EEA1)* (generous gift from S. Field) and subcloned into the pRS305 vector by *Xho*II/*Sac*I. This plasmid was linearized using *Afl*II and integrated into the *LEU2* locus. Similarly, the *FAPP1-PH-Cyc1*$_{term}$ sequence was subcloned from *pRS306-mCherry-FAPP1-PH* (NRB1444) (Mizuno-Yamasaki *et al.*, 2010) into the *YIplac128-pADH1-mCherry* vector by *Bam*HI/*Eag*I. This plasmid (NRB1705) was linearized using *Afl*II and integrated into the *LEU2* locus. To generate the HemiZap vector *pRS305-mup1-GFP* (NRB1701), first a fragment containing GFP and the *Cyc1* terminator was excised from NRB1685 with *Nhe*I and *Not*I and used to replace the mCherry-Cyc1$_{term}$ part in NRB1699 (*pRS305-vps8-mcherryx6*) and then a C-terminal fragment of *Mup1* (740–1723 base pairs) was amplified by PCR and subcloned into the above plasmid with *Sal*I and *Nhe*I. This plasmid was linearized with *Bsu36*I and transformed into yeast at the *MUP1* locus.

All the other yeast strains were constructed by recombination to delete the gene or tag the gene chromosomally (Longtine *et al.*, 1998) or by a genetic cross to select a haploid of the appropriate genotype.

Growth test

Yeast cells were grown overnight in yeast peptone dextrose (YPD) or synthetic complete (SC) dropout medium to stationary phase. Cells were washed once with sterile water and spotted on YPD or SC dropout plates in fivefold serial dilutions starting with an OD_{600} of 0.2. For GAL induction experiments, yeast cells were grown in YP medium containing 2% raffinose overnight and then spotted on YP-GAL plates. Plates were incubated at the specified temperature for the indicated time.

Cell lysate extracts and immunoblotting

Yeast cells were grown to OD_{600} ~ 1 at 25°C. For each strain equal numbers of cells were harvested and lysed by a rapid alkaline lysis procedure as previously described (Westfall *et al*., 2008). Proteins were subjected to Western blot analysis with mouse monoclonal anti-GFP antibody (1:2000 dilution; Roche), rabbit polyclonal anti-Sec2 antibody (1:2000 dilution; lab made), or mouse monoclonal anti-Pgk1(phosphoglycerate kinase) antibody as loading control (1:5000 dilution; Invitrogen).

Bgl2 secretion assay

The Bgl2 secretion assay was performed as described by Kozminski *et al*. (2006) with minor modification. In brief, yeast cells (20 ml) were grown at 25°C in YPD overnight to early log phase (0.4–0.8 OD_{600}/ml). About 5 OD_{600} units of cells were harvested by centrifugation at 900 × *g* for 5 min. Three different sets of cultures were prepared for each strain. Cell pellets were resuspended in 1 ml of ice-cold 10 mM NaN_3 and 10 mM NaF, followed by a 10-min incubation on ice. The suspension was transferred to microfuge tubes, pelleted, and resuspended in 1 ml of fresh prespheroplasting buffer (100 mM Tris-HCl, pH 9.4, 50 mM β-mercaptoethanol, 10 mM NaN_3, and 10 mM NaF). After a 15-min incubation on ice, cells were pelleted and washed with 0.5 ml of spheroplast buffer (50 mM KH_2PO_4-KOH, pH 7.0, 1.4 M sorbitol, and 10 mM NaN_3). Cells were resuspended in 1 ml of spheroplast buffer containing 167 µg/ml zymolyase 100T (Nacasai Tesque). Cells were incubated in a 37°C water bath for 30 min. Spheroplasts were then pelleted at 5000 × *g* for 10 min, and 100 µl of the supernatant was transferred into a new tube and mixed with 50 µl of 3× SDS sample buffer. This represents the external pool. All the remaining supernatant was removed, and the spheroplast pellet was rinsed once with 1 ml of spheroplast buffer and then resuspended in 100 µl of 2× SDS sample buffer. This represents the internal pool. Proper amounts of each internal pool sample and external pool sample were loaded onto a 12% SDS–PAGE gel. Bgl2 was visualized by Western blotting with anti-Bgl2 rabbit polyclonal antibody at 1:5000 dilution (provided by R. Schekman, University of California, Berkeley). The amount of Bgl2 in both internal and external pools was determined by ImageJ software. The fraction of internal Bgl2 accumulated was calculated by Int/(Int + Ext).

Electron microscopy

Yeast cells expressing full-length Sec2-GFP or Sec2GEF-GFP-CUE from the *ADH1* promoter in the *sro7*Δ*::LEU2* background (NY3398 and NY3395) as well as control cell *sro7*Δ*::LEU2* (NY2599) were grown at 25°C in YPD to an $OD_{600\,nm}$ of ~0.5 and then processed for EM as previously described (Chen *et al*., 2012). Alternatively, yeast cells expressing full-length Sec2-GFP or Sec2GEF-GFP-CUE from the *ADH1* promoter in the wild-type background (NY3384 and NY3381) were grown at 25°C in YPD to an $OD_{600\,nm}$ of ~0.5 and EM was performed as described (Cui *et al*., 2019). Briefly, cells were fixed in potassium permanganate and embedded in Spurr's resin. After polymerization, 55- to 60-nm thin sections were cut using an Ultracut ultramicrotome (Leica Microsystems), transferred onto formvar carbon–coated copper grids, and stained before viewing. For both preparation conditions, the images were acquired using a transmission electron microscope (Tecnai G2 Spirit; FEI) equipped with a CCD camera (UltraScan 4000; Gatan).

Fluorescence microscopy and quantitative localization analysis

Yeast strains harboring GFP, mCherry, or dsRed tags were grown overnight to early log phase (OD_{600} 0.4–0.6) in selective SC medium at 25°C. Live cells (500 µl) were pelleted by centrifugation at 5000 rpm for 1 min and resuspended in 50 µl of medium. Cell suspension (5 µl) was spotted on a glass slide with coverslip. The cells were examined on two different microscopes, typically on an Axiophot 2 upright microscope (Carl Zeiss Microimaging) with a 100× Plan apochromatic oil-immersion objective lens with NA 1.3 and 100 W xenon excitation lamp and with a cool-CCD camera (model ORCA ER; Hamamatsu). As specified, some fluorescence images were acquired on a Yokagawa spinning-disk confocal microscopy system (Zeiss Carl Observer Z1) with a 100× oil immersion objective lens (Plan Apochromat 100×/1.4 NA oil differential interference contrast (DIC) lens; Carl Zeiss) equipped with an electron-multiplying CCD camera (QuantEM 512SC; Photometrics). Excitation of GFP or mCherry/dsRed was achieved using 488-nm argon and 568-nm argon/krypton lasers, respectively. For each sample, a z-stack with a 200-nm slice distance was generated. Images were analyzed using velocity or AxioVision software 4.8 (Carl Zeiss).

To quantify the localization of Sec2 or Sec2GEF-CUE, ~50 cells were examined for each condition and at least three independent clones were tested for each strain to calculate the SD. When the GFP/mCherry signal was mainly detected at the tips of small/medium budded cells and at the bud necks of large-budded cells, these cells were scored as polarized; otherwise, when the GFP/mCherry signal was mainly detected as puncta inside the cytosol, away from the bud tip or bud neck area, these cells were scored as nonpolarized. Those that contained mostly diffuse GFP or mCherry signal were not counted.

Time-lapse imaging and analysis of Sec2 or Sec2GEF-CUE containing vesicles

The time-lapse fluorescence imaging was conducted on yeast strains expressing full-length Sec2-NeonGreen or Sec2GEF-NeonGreen-CUE. Cells were grown overnight in SC medium to early log phase (0.3–0.5 OD_{600}) and then were applied to a 35-mm MatTek dish (Ashland) pretreated with 0.05 mg/ml concanavalin A (EY Laboratories) for imaging on a Yokogawa W1-SoRa spinning–disk confocal mounted on a Nikon Ti2-E microscope body. Images were acquired with a 100× Plan Apo Lambda 1.35 NA silicone immersion objective. A Nikon LUNF-XL six-line (405, 445, 488, 520, 561, and 640 nm) laser engine, Prime 95B back-thinned sCMOS camera (Teledyne Photometrics), and piezo Z-stage (Mad City Labs) were used to acquire images via NIS Elements software. Images were taken with the SoRa mode with 2.8× additional magnification, 100 ms exposure time, and 20–40% 488-nm laser power. To train an AI enhancement model with the enhance.ai module in NIS Elements software, a set of more than 100 image pairs of these cells were acquired, with the first image acquired with the above imaging settings with the second acquired with 80% 488-nm laser power and 150 ms exposure time. Training of the AI model proceeded to a training loss of 0.136, which was largely due to the fact that there

was movement between the two image frames as the sample was unfixed. The enhance.ai model was incorporated into a GA3 workflow, which allowed us to batch apply it to all images.

Individual vesicles that have the expected intensity and display a clear moving track were identified by eye. The lifetime for vesicle puncta was quantified by kymograph in ImageJ v2.1. Briefly, a time-lapse image was max-projected in time to create a new image in which the movement of individual vesicles could be detected as lines. These lines were traced and added to the region of interest (ROI) manager. In the ROI Manager, selected segmented lines were placed in the original image stacks and then the Reslice Stack command was used to obtain kymograph images of the objects, where the *y*-axis distance represents the lifetime of the vesicles. Owing to the time duration of the imaging, some of the vesicles tracked remained visible until the end of imaging, and therefore the lifetimes were grouped into three ranges; the vesicle dynamics can be compared by their distribution within the different ranges.

FRAP experiment and image analysis

The live-cell preparation and time-lapse imaging after photobleaching for fluorescence recovery after photobleach (FRAP) experiments were conducted with the same spinning-disk confocal microscope system as described above. Photobleaching of the entire bud was performed using an OptiMicroScan X-Y Galvo system with a 1-ms dwell time, and the laser intensity was set to 10% from a directly coupled 20 mW, 405-nm laser. The bleach duration was chosen by determining the minimal time needed to completely bleach the fluorescent signal. To increase imaging speed and avoid photobleaching, images were taken using a 256 × 256 pixel ROI. Three prebleached images were acquired without a delay, and postbleaching images were taken continuously for 30 s and then with 1 s intervals for a subsequent 1 min. In the vesicle-tracking experiments after photobleaching, the movies were taken in a z stack of five planes (covering 2.5 µm), each with 100 ms exposure time from 20- to 40% 488-nm laser power.

ROIs for the bleached bud and the whole cell as well as a rectangular background ROI in a dark extracellular region were drawn by hand and moved into the ROI Manager. The Time Measurement tool within NIS Elements was used to quantify the intensity of the bleached ROIs as well as the entire cell after the background intensity was subtracted from the images. The fluorescence recovery within the bleached bud relative to the total signal within the whole cell was plotted over time, and the prebleached signal intensity was normalized as 100%. The pixel intensity changes of a nonbleached cell over time were collected to adjust for the photobleaching effects of imaging.

Sec2-NeonGreen– or Sec2GEF-NeonGreen-CUE–positive vesicles entering the bud after FRAP were tracked by eye until one was observed tethering to the plasma membrane or relatively stabilized around the plasma membrane area. Only those vesicles free of adjacent vesicles or overlapping vesicles throughout the tracking time were analyzed. If the vesicles disappeared from plasma membrane sites, we checked in other z-stack planes to confirm that they vanished due to fusion and not due to drift out of the field of view in the z direction. Static images were converted to 16 bits and displayed in inverted monochrome maximum projection and then range adjusted to the minimum and maximum contrast with ImageJ. Owing to the dramatic dynamic difference of vesicles in wild-type Sec2-NeonGreen and Sec2GEF-NeonGreen-CUE cells and the relatively low intensity of vesicles, kymograph by line around bud cortex in NIS software showed large variations. Quantitation of the time from appearance to disappearance for individual vesicle puncta was obtained manually for more than 20 cells for each strain.

Endocytosis of Mup1-GFP and image quantitation

To track endocytosis, we integrated the GFP sequence at the C-terminus of Mup1 in wild-type, *SEC2-mCherry,* or *SEC2GEF-mCherry-CUE* strains. Cells were grown overnight to early log phase (0.3–0.5 OD_{600}) in SC medium without methionine and were applied to a 35-mm MatTek dish pretreated with 0.05 mg/ml concanavalin A. Cells were quickly rinsed with SC medium without methionine, and then fresh SC medium containing methionine was added to stimulate endocytosis before conducting time-lapse imaging on a Yokogawa X1 spinning-disk confocal system attached to a Ti2-E. The Nikon microscope employed was equipped with a 100× Apo total internal reflection fluorescence (TIRF) 1.49 NA objective, a Prime 95B back-thinned sCMOS camera, and NIS Elements software. Acquisition settings for Mup1-GFP endocytosis were 60-min duration, 1-min interval time, 200-ms exposure time, 20% 488-nm laser power, one *z*-axis plane with Nikon perfect focus system (PFS) setting to prevent drifting. The temperature of the immersion oil on the microscopy slide near the sample was ~24°C.

Image processing and quantitation were performed using the provided NIS Elements software. Rectangular ROIs in the cell plasma membrane were drawn manually to exclude any obvious puncta from inside or next to the ROIs. The Time Measurement tool within NIS Elements was used to quantify the intensity of the plasma membrane in all selected ROIs, and then results were exported to Excel. The intensity at the starting time point was set as 100%, and then the percentage of Mup1-GFP intensity residing on the plasma membrane was plotted over time. At least three independent experiments were performed, and a minimum of 50 yeast cells were quantified from each experiment. The averaged intensity decrease for one representative experiment is shown. Best-fit exponential trend lines with second-order decay were applied, and a τ value, half-life of Mup1-GFP on plasma membrane, was determined. The averaged τ values for Mup1-GFP in *SEC2-mCherry* or *SEC2GEF-mCherry-CUE* were from at least three endocytosis experiments. Probability values (*P* value) were calculated using the Student's *t* test, and all comparisons with a P value < 0.005 were considered statistically significant.

The quantitation of cell percentage containing GFP signal in the vacuole was done manually at two time points, 63 and 93 min after the addition of methionine. The time-lapse imaging was acquired on a Yokagawa spinning-disk confocal microscopy system (Zeiss Carl Observer Z1) equipped with a 100× oil immersion objective lens, an electron-multiplying CCD camera (QuantEM 512SC; Photometrics), and AxioVision software 4.8 (Carl Zeiss). Acquisition settings for Mup1-GFP endocytosis were 90-min duration, 15-min interval time, 200-ms exposure time, 80% 488-nm laser power, and a z stack of five planes with a step of 0.25 µm. Three independent experiments were performed, and a minimum number of 30 yeast cells were quantified from each experiment.

ACKNOWLEDGMENTS

This work was supported by grants GM35370 and GM08261 to P. N. from the National Institutes of Health and by the George E. Palade Endowed Chair and Margret Shaw Roberts Fund. We thank Randy Schekman, University of California at Berkeley, Nan Hao, University of California at San Diego, Seth Field, Case Western Reserve University, and Benjamin Glick, University of Chicago, for reagents. We also thank Hua Yuan and David Shen for their assistance in strain construction.

REFERENCES

Aivazian D, Serrano RL, Pfeffer S (2006). TIP47 is a key effector for Rab9 localization. J Cell Biol 173, 917–926.

Araki S, Kikuchi A, Hata Y, Isomura M, Takai Y (1990). Regulation of reversible binding of smg p25A, a ras p21-like GTP-binding protein, to synaptic plasma membranes and vesicles by its specific regulatory protein, GDP dissociation inhibitor. J Biol Chem 265, 13007–13015.

Blumer J, Rey J, Dehmelt L, Mazel T, Wu YW, Bastiaens P, Goody RS, Itzen A (2013). RabGEFs are a major determinant for specific Rab membrane targeting. J Cell Biol 200, 287–300.

Boyd C, Hughes T, Pypaert M, Novick P (2004). Vesicles carry most exocyst subunits to exocytic sites marked by the remaining two subunits, Sec3p and Exo70p. J Cell Biol 167, 889–901.

Brennwald P, Kearns B, Champion K, Keranen S, Bankaitis V, Novick P (1994). Sec9 is a SNAP-25-like component of a yeast SNARE complex that may be the effector of Sec4 function in exocytosis. Cell 79, 245–258.

Cabrera M, Ungermann C (2013). Guanine nucleotide exchange factors (GEFs) have a critical but not exclusive role in organelle localization of Rab GTPases. J Biol Chem 288, 28704–28712.

Chen S, Novick P, Ferro-Novick S (2012). ER network formation requires a balance of the dynamin-like GTPase Sey1p and the Lunapark family member Lnp1p. Nat Cell Biol 14, 707–716.

Cui Y, Parashar S, Zahoor M, Needham PG, Mari M, Zhu M, Chen S, Ho HC, Reggiori F, Farhan H, *et al*. (2019). A COPII subunit acts with an autophagy receptor to target endoplasmic reticulum for degradation. Science 365, 53–60.

Day KJ, Casler JC, Glick BS (2018). Budding yeast has a minimal endomembrane system. Dev Cell 44, 56–72.e54.

Dong G, Medkova M, Novick P, Reinisch KM (2007). A catalytic coiled coil: structural insights into the activation of the Rab GTPase Sec4p by Sec2p. Mol Cell 25, 455–462.

Donovan KW, Bretscher A (2015). Tracking individual secretory vesicles during exocytosis reveals an ordered and regulated process. J Cell Biol 210, 181–189.

Elkind NB, Walch-Solimena C, Novick PJ (2000). The role of the COOH terminus of Sec2p in the transport of post-Golgi vesicles. J Cell Biol 149, 95–110.

Finger FP, Hughes TE, Novick P (1998). Sec3p is a spatial landmark for polarized secretion in budding yeast. Cell 92, 559–571.

Grosshans BL, Andreeva A, Gangar A, Niessen S, Yates JR 3rd, Brennwald P, Novick P (2006a). The yeast lgl family member Sro7p is an effector of the secretory Rab GTPase Sec4p. J Cell Biol 172, 55–66.

Grosshans BL, Ortiz D, Novick P (2006b). Rabs and their effectors: achieving specificity in membrane traffic. Proc Natl Acad Sci USA 103, 11821–11827.

Guiney EL, Klecker T, Emr SD (2016). Identification of the endocytic sorting signal recognized by the Art1-Rsp5 ubiquitin ligase complex. Mol Biol Cell 27, 4043–4054.

Guo W, Roth D, Walch-Solimena C, Novick P (1999). The exocyst is an effector for Sec4p, targeting secretory vesicles to sites of exocytosis. EMBO J 18, 1071–1080.

Hama H, Tall GG, Horazdovsky BF (1999). Vps9p is a guanine nucleotide exchange factor involved in vesicle-mediated vacuolar protein transport. J Biol Chem 274, 15284–15291.

Horiuchi H, Lippé R, McBride HM, Rubino M, Woodman P, Stenmark H, Rybin V, Wilm M, Ashman K, Mann M, Zerial M (1997). A novel Rab5 GDP/GTP exchange factor complexed to rabaptin-5 links nucleotide exchange to effector recruitment and function. Cell 90, 1149–1159.

Hutagalung AH, Coleman J, Pypaert M, Novick PJ (2009). An internal domain of Exo70p is required for actin-independent localization and mediates assembly of specific exocyst components. Mol Biol Cell 20, 153–163.

Hutagalung AH, Novick PJ (2011). Role of Rab GTPases in membrane traffic and cell physiology. Physiol Rev 91, 119–149.

Jin Y, Sultana A, Gandhi P, Franklin E, Hamamoto S, Khan AR, Munson M, Schekman R, Weisman LS (2011). Myosin V transports secretory vesicles via a Rab GTPase cascade and interaction with the exocyst complex. Dev Cell 21, 1156–1170.

Kozminski KG, Alfaro G, Dighe S, Beh CT (2006). Homologues of oxysterol-binding proteins affect Cdc42p- and Rho1p-mediated cell polarization in Saccharomyces cerevisiae. Traffic 7, 1224–1242.

Lehman K, Rossi G, Adamo JE, Brennwald P (1999). Yeast homologues of tomosyn and lethal giant larvae function in exocytosis and are associated with the plasma membrane SNARE, Sec9. J Cell Biol 146, 125–140.

Lewis MJ, Nichols BJ, Prescianotto-Baschong C, Riezman H, Pelham HR (2000). Specific retrieval of the exocytic SNARE Snc1p from early yeast endosomes. Mol Biol Cell 11, 23–38.

Ling Y, Hayano S, Novick P (2014). Osh4p is needed to reduce the level of phosphatidylinositol-4-phosphate on secretory vesicles as they mature. Mol Biol Cell 25, 3389–3400.

Liu D, Novick P (2014). Bem1p contributes to secretory pathway polarization through a direct interaction with Exo70p. J Cell Biol 207, 59–72.

Longtine MS, McKenzie A 3rd, Demarini DJ, Shah NG, Wach A, Brachat A, Philippsen P, Pringle JR (1998). Additional modules for versatile and economical PCR-based gene deletion and modification in Saccharomyces cerevisiae. Yeast 14, 953–961.

Losev E, Reinke C, Jellen J, Strongin D, Bevis B, Glick B (2006). Golgi maturation in living yeast. Nature 441, 1002–1006.

Medkova M, France YE, Coleman J, Novick P (2006). The rab exchange factor Sec2p reversibly associates with the exocyst. Mol Biol Cell 17, 2757–2769.

Mizuno-Yamasaki E, Medkova M, Coleman J, Novick P (2010). Phosphatidylinositol 4-phosphate controls both membrane recruitment and a regulatory switch of the Rab GEF Sec2p. Dev Cell 18, 828–840.

Mizuno-Yamasaki E, Rivera-Molina F, Novick P (2012). GTPase networks in membrane traffic. Annu Rev Biochem 81, 637–659.

Nagano M, Toshima JY, Siekhaus DE, Toshima J (2019). Rab5-mediated endosome formation is regulated at the trans-Golgi network. Commun Biol 2, 419.

Nottingham RM, Pusapati GV, Ganley IG, Barr FA, Lambright DG, Pfeffer SR (2012). RUTBC2 protein, a Rab9A effector and GTPase-activating protein for Rab36. J Biol Chem 287, 22740–22748.

Ortiz D, Medkova M, Walch-Solimena C, Novick P (2002). Ypt32 recruits the Sec4p guanine nucleotide exchange factor, Sec2p, to secretory vesicles; evidence for a Rab cascade in yeast. J Cell Biol 157, 1005–1015.

Peterson MR, Burd CG, Emr SD (1999). Vac1p coordinates Rab and phosphatidylinositol 3-kinase signaling in Vps45p-dependent vesicle docking/fusion at the endosome. Curr Biol 9, 159–162.

Pusapati GV, Luchetti G, Pfeffer SR (2012). Ric1-Rgp1 complex is a guanine nucleotide exchange factor for the late Golgi Rab6A GTPase and an effector of the medial Golgi Rab33B GTPase. J Biol Chem 287, 42129–42137.

Rana M, Lachmann J, Ungermann C (2015). Identification of a Rab GTPase-activating protein cascade that controls recycling of the Rab5 GTPase Vps21 from the vacuole. Mol Biol Cell 26, 2535–2549.

Rivera-Molina FE, Novick PJ (2009). A Rab GAP cascade defines the boundary between two Rab GTPases on the secretory pathway. Proc Natl Acad Sci USA 106, 14408–14413.

Salminen A, Novick PJ (1989). The Sec15 protein responds to the function of the GTP binding protein, Sec4, to control vesicular traffic in yeast. J Cell Biol 109, 1023–1036.

Seabra MC, Mules EH, Hume AN (2002). Rab GTPases, intracellular traffic and disease. Trends Mol Med 8, 23–30.

Shen D, Yuan H, Hutagalung A, Verma A, Kummel D, Wu X, Reinisch K, McNew JA, Novick P (2013). The synaptobrevin homologue Snc2p recruits the exocyst to secretory vesicles by binding to Sec6p. J Cell Biol 202, 509–526.

Shideler T, Nickerson DP, Merz AJ, Odorizzi G (2015). Ubiquitin binding by the CUE domain promotes endosomal localization of the Rab5 GEF Vps9. Mol Biol Cell 26, 1345–1356.

Stalder D, Mizuno-Yamasaki E, Ghassemian M, Novick PJ (2013). Phosphorylation of the Rab exchange factor Sec2p directs a switch in regulatory binding partners. Proc Natl Acad Sci USA 110, 19995–20002.

Suda Y, Kurokawa K, Hirata R, Nakano A (2013). Rab GAP cascade regulates dynamics of Ypt6 in the Golgi traffic. Proc Natl Acad Sci USA 110, 18976–18981.

Walch-Solimena C, Collins RN, Novick PJ (1997). Sec2p mediates nucleotide exchange on Sec4p and is involved in polarized delivery of post-Golgi vesicles. J Cell Biol 137, 1495–1509.

Walch-Solimena C, Novick P (1999). The yeast phosphatidylinositol-4-OH kinase pik1 regulates secretion at the Golgi. Nat Cell Biol 1, 523–525.

Westfall PJ, Patterson JC, Chen RE, Thorner J (2008). Stress resistance and signal fidelity independent of nuclear MAPK function. Proc Natl Acad Sci USA 105, 12212–12217.

Whyte JR, Munro S (2002). Vesicle tethering complexes in membrane traffic. J Cell Sci 115, 2627–2637.

Zhu H, Liang Z, Li G (2009). Rabex-5 is a Rab22 effector and mediates a Rab22-Rab5 signaling cascade in endocytosis. Mol Biol Cell 20, 4720–4729.